

Spatial - Temporal Analysis of Vegetation Cover Dynamics Following Cyclone Freddy: A Case Study of Blantyre, Malawi.

Ganetie Assabie

GIS-002-20

Thyolo Malawi

Dissertation Submitted in Partial Fulfillment of the Requirements

for the Award of the Bachelor of Science Degree in Geo-

Information and Earth Observation Science

Malawi University of Science and Technology

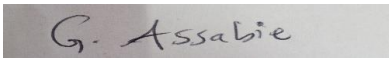
Ndata School Of Climate and Earth Science Department of Earth

Sciences

DATE: 29TH April, 20

DECLARATION

I Ganetie Assabie confirm that the research project "**Spatial - Temporal Analysis of Vegetation Cover Dynamics Following Cyclone Freddy: A Case Study of Blantyre, Malawi.**" is my work. I have never submitted it to any other institution for academic purposes. Any information I have used or mentioned from other sources has been properly credited with complete references.

Signature: 

DISSERTATION APPROVED BY:

SUPERVISOR:

Dr. J Nyengere **Signature:** 

ASSESSOR:

Signature: _____

DISCLAIMER

This document describes work undertaken as part of a program of study at Ndata School of Climate and Earth Sciences of the Malawi University of Science and Technology. All views and opinions expressed therein remain the sole responsibility of the author(s), and do not necessarily represent those of the school.

COPYRIGHT STATEMENT:

This copy of the dissertation has been supplied on condition that anyone who consults it is understood to recognize that its copyright rests with its author and that no quotation from the dissertation and no information derived from it may be published without acknowledgement.

Abstract

Cyclone Freddy, a severe tropical storm, struck the Southern Region of Malawi in March 2023 causing extensive environmental damage, Blantyre was one of the affected districts. This dissertation focuses on assessing the cyclone's impact on vegetation cover through geospatial analysis, with the aim of enhancing understanding of ecological resilience following extreme weather events. The study employed high-resolution Sentinel-2 Multispectral Instrument imagery and applied the Normalized Difference Vegetation Index (NDVI) technique to detect vegetation loss across four selected areas within Blantyre: Nyambadwe, Ndirande, Chilomoni, and Soche-Chilobwe. Data processing and analysis were conducted using Google Earth Engine (GEE), ArcMap, and QGIS platforms. NDVI differencing was used to map spatial and temporal vegetation dynamics before and after the cyclone. Results indicated significant declines in vegetation health, with Ndirande and Chilomoni experiencing the most pronounced degradation, while some resilience and regrowth were observed in parts of Soche and Nyambadwe. The findings underscore the impact of Cyclone Freddy, influenced by topographic and urbanization factors. It is recommended that future resilience-building efforts integrate high-resolution vegetation monitoring and ground-truth validation to support disaster preparedness and sustainable land management planning. The methodology presented can serve as a model for future studies assessing post-disaster ecological impacts in cyclone-prone regions.

Keywords: Cyclone Freddy, NDVI, Sentinel-2, Vegetation Change Detection, Google Earth Engine, Blantyre City, Remote Sensing

ACKNOWLEDGEMENTS

First of all, I would like to thank Elohim God, who made it possible to begin and finish this work successfully. Many individuals have assisted me in one way or another, and although it is difficult to mention each one by name, I sincerely extend my heartfelt appreciation to all. Nonetheless, it is important to recognize a few individuals whose dedicated support and contributions were instrumental from the initial stages of title formulation to the completion of the write-up.

I would like to express my sincere gratitude to my supervisor, Dr. J. Nyengere for his invaluable technical support, guidance, and encouragement throughout the research period. My heartfelt thanks also go to my family and friends for their unwavering financial and emotional support, which sustained me throughout this journey, with special appreciation to my aunt, Magret Mkandawire, for her continuous emotional encouragement. I am equally grateful to Lucious Malalu for his invaluable assistance in providing data and essential information regarding the study area.

I am also thankful to my classmates for their cooperative interactions and exchange of educational materials.

This achievement would not have been possible without the collective contributions of these individuals and many others. Their support has been truly invaluable, and for that, I remain deeply grateful. May Elohim God bless and keep you all abundantly.

Table of Contents

DECLARATION i
DISCLAIMER ii
COPYRIGHT STATEMENT: iii
Abstract iv
ACKNOWLEDGEMENTS v
ACRONYMS AND ABBREVIATIONS viii
CHAPTER 1: INTRODUCTION 1
1.1 BACKGROUND: 1
1.2 PROBLEM STATEMENT 3
1.3 MAIN AND SPECIFIC OBJECTIVES 3
1.31 Main Objective: 3
1.32 Specific Objectives: 3
1.4 RESEARCH QUESTIONS 4
1.5 SIGNIFICANCE OF THE STUDY 4
CHAPTER 2: LITERATURE REVIEW 6
2.1 Tropical Cyclone Freddy in Malawi and its impact on Malawian communities. 6
2.2 Areas within Blantyre that have been markedly influenced by Cyclone Freddy 7
2.3 Cyclone Freddy vs Vegetation and Land cover 7
2.4 Factors Influencing Vegetation Resilience 8
2.5 Spatial Distribution of Vegetation Loss and Recovery in Areas 8
2.6 Remote Sensing in Disaster Assessment 9
2.7 Spatial-Temporal Techniques in Cyclone Impact Assessment 9
2.8 Cyclone Freddy-Specific Studies in Malawi 10
2.9 Gaps in Current Research 10
CHAPTER 3: METHODOLOGY 11
3.1 Research Design 11
3.2 Materials and methods 12
3.2.1 Study Area: 12
3.2.2 Earth Observations Data: 14

3.3.4 Sentinel-2 Imagery Processing 18
CHAPTER 4: RESULTS AND DISCUSSION 19
4.1 Temporal NDVI Changes for AOI Within Blantyre 19
4.1.1 NYAMBADWE 19
4.1.2 CHILOMONI 21
4.1.3 Soche and Chilobwe regions 23
4.1.4 NDIRANDE 25
CHAPTER 5: CONCLUSIONS AND RECOMMENDATIONS 29
5.1 Conclusion 29
5.2 Recommendations 30
CHAPTER 6: REFERENCES 31
APPENDICES 35
Appendix A: GEE Codes for Data Collection and NDVI Calculations 35
Appendix B: ArcMap Raster Calculator Expression for NDVI Change Detection 46
Appendix C: Summary of Satellite Data Collection Parameters 47

ACRONYMS AND ABBREVIATIONS

AOI: Area of Interest

DoDMA: Department of Disaster Management Affairs

EMS: Electromagnetic Spectrum

ENSO: El Niño-Southern Oscillation

FVC: Fractional Vegetation Cover

GEE: Google Earth Engine

GIS: Geographic Information System

MSI: Multispectral Instrument

NDVI: Normalized Difference Vegetation Index

SPOT: Satellite Pour l'Observation de la Terre

SSR: Surface Solar Radiation

VPD: Vapor Pressure Deficit

LIST OF FIGURES

Figure 1: The devastation caused by Cyclone Freddy under Mount Soche in Blantyre (Photos courtesy Tim Lawrence((Baresford, 2023) 2
Figure 2: Residents survey the damage caused by Cyclone Freddy in Chilobwe, Blantyre, Malawi, March 13, 2023. REUTERS/Eldson Chagara (Kabukuru & Gondwe, 2023) 3
Figure 3: Methodology flowchart followed during research. 12
Figure 4: Map of Blantyre depicting areas of Focus: Ndirande, Nyambadwe, Soche_Chilobwe and Chilomoni..... 14
Figure 5: Workflow of NDVI method. 16
Figure 6: NDVI map for Nyambadwe depicting for both pre and post periods 19
Figure 7: Change detection Map for Nyambadwe 20
Figure 8: NDVI map for Chilomoni depicting for both pre and post periods..... 21
Figure 9: Change detection map for Chilomoni 22
Figure 10: NDVI map for Soche_Chilobwe depicting for both pre and post periods 23
Figure 11: Change detection Map for Soche_Chilobwe 24
Figure 12: NDVI map for Ndirande depicting for both pre and post periods 25
Figure 13: Change detection Map for Ndirande 26

LIST OF TABLES

Table 1: Before Cyclone Freddy (October 2022) 15
Table 2 : After Cyclone Freddy (October 2023) 15
Table 3: Classification schema for vegetation cover. (Shabab et al., 2025)(Hoque, 2017) 17
Table 4: Summary of NDVI Results for Study Areas 27
Table 5:Summary of Change Detection Analysis for Study Areas 28

CHAPTER 1: INTRODUCTION

1.1 BACKGROUND:

Tropical cyclones are among the most destructive and life-threatening natural disasters globally, especially in coastal and low-lying areas (Akter & Dayem, 2021). Hydro-meteorological phenomena develop over warm tropical oceans and are classified as cyclones, typhoons, or hurricanes based on their geographical location (Hoque, 2017). Their destructive force generally results from intense and sustained winds, heavy rainfall, storm surges, and extensive coastal inundation, all of which present significant threats to human populations and natural ecosystems (Akter & Dayem, 2021).

The impacts of tropical cyclones in Sub-Saharan Africa are intensifying, especially in the context of increasing climate variability. Parts of the region, particularly southeastern Africa, have seen an increase in cyclone activity in recent years, resulting in significant environmental degradation, displacement, and loss of biodiversity (Mpheza, 2023b). Mozambique, Madagascar, and Malawi have experienced recurrent cyclone events, highlighting their environmental vulnerability and inadequate disaster preparedness (Editor José Paula et al., 2023).

Cyclone Freddy made landfall in Malawi in March 2023, resulting in significant devastation, especially in the Southern Region. Torrential rains resulted in landslides, flooding, and extensive damage to infrastructure and vegetation, displacing hundreds of thousands (Study, 2023). The geospatial mapping exercise conducted post-disaster by the Scotland Malawi Partnership indicated that several districts, including Mulanje, Machinga, and Zomba, suffered significant vegetation damage (Kadzuwa & Partnership, 2023). The significant reduction in green cover, serving as an indicator of cyclone impact, underscores the vulnerability of Malawi's ecosystems to climate disturbances.

Blantyre District, located in Malawi's Southern Region, was one of the areas impacted by Cyclone Freddy in March 2023 (Kadzuwa & Partnership, 2023). Blantyre encountered disruptions, especially in its urban and elevated areas. The cyclone's significant rainfall and

intense winds presented risks of flooding, landslides, and vegetation stress in certain areas of the district (Mpheza, 2023). The events illustrate the increasing environmental susceptibility of urban areas such as Blantyre to extreme weather phenomena and emphasize the necessity for localized evaluations of ecological resilience.

Understanding the effects of Cyclone Freddy on plant growth patterns is essential for enhancing environmental resilience and preparedness in cyclone-affected areas (Hoenigl et al., 2022). By addressing this gap in understanding, policymakers and key stakeholders can formulate more effective strategies for disaster management and develop plans for sustainable development. This investigation focuses on a detailed analysis of the impact of Cyclone Freddy on vegetative resilience and coverage in Blantyre, Malawi, utilizing geographical and temporal data.



Figure 1: The devastation caused by Cyclone Freddy under Mount Soche in Blantyre (Photos courtesy Tim Lawrence((Baresford, 2023)



Figure 2: Residents survey the damage caused by Cyclone Freddy in Chilobwe, Blantyre, Malawi, March 13, 2023. REUTERS/Eldson Chagara (Kabukuru & Gondwe, 2023)

1.2 PROBLEM STATEMENT

Cyclone Freddy (Mpheza, 2023) resulted in vegetation loss in Blantyre (Kadzuwa & Partnership, 2023). However, significant questions remain regarding the temporal and spatial patterns of ecosystem recovery. Previous research indicates that forests and biodiversity suffer immediate damage (Issn, 2023; Kadzuwa & Partnership, 2023). However, there is a notable absence of high-resolution, terrain-sensitive analyses regarding post-cyclone vegetation dynamics. Addressing this gap is crucial for enhancing environmental resilience and preparedness in cyclone-affected regions, thereby informing the development of sustainable plans and effective disaster management strategies.

1.3 MAIN AND SPECIFIC OBJECTIVES

1.31 Main Objective:

To conduct a temporal-spatial analysis of vegetation cover in areas affected by Cyclone Freddy, focusing on Blantyre, Malawi.

1.32 Specific Objectives:

1. To identify areas significantly affected by Cyclone Freddy in Blantyre.
2. To assess the temporal changes in vegetative cover before and after Cyclone Freddy.

3. To examine the spatial distribution of vegetation loss and recovery in areas surrounding hills.

1.4 RESEARCH QUESTIONS

1. Which areas within Blantyre were most significantly affected by Cyclone Freddy in terms of vegetation cover?
2. How did vegetation cover change temporally before and after the occurrence of Cyclone Freddy?
3. What is the spatial distribution pattern of vegetation degradation and regrowth, particularly around hilly and elevated terrains in the affected regions?

1.5 SIGNIFICANCE OF THE STUDY

This study focuses on the impact of Cyclone Freddy on vegetation cover in Blantyre, Malawi. This study aims to elucidate the temporal-spatial dynamics of vegetation in areas affected by cyclones and to demonstrate the resilience of natural ecosystems to catastrophic weather events. Understanding the impact of Cyclone Freddy on vegetation is essential for enhancing environmental resilience and preparedness in cyclone-prone areas. This study seeks to address significant knowledge gaps regarding the environmental impacts of cyclones and to enhance the development of effective disaster management strategies.

While previous studies have illuminated the impact of cyclones on ecosystems, further investigation is necessary to understand the specific effects on resilience and vegetation cover. This study aims to address the gap by conducting a comprehensive investigation of vegetation dynamics in areas impacted by Cyclone Freddy. The objective is to enhance the existing knowledge in the field and improve understanding of the relationships between extreme weather events and natural ecosystems through the analysis of temporal and geographical patterns of plant cover before and after the cyclone.

This study's results have important implications for enhancing environmental resilience and managing disasters in cyclone-affected regions. Policymakers and stakeholders can

enhance disaster planning and response by identifying regions significantly affected by Cyclone Freddy and analyzing factors influencing vegetation resilience. The insights gained from this study can inform sustainable development and land-use planning initiatives, ultimately enhancing the long-term resilience of ecosystems and communities in Blantyre and its vicinity.

Local governments, environmental organizations, and legislators engaged in disaster management and land-use planning in cyclone-prone regions may find the study's findings particularly beneficial. This research aims to improve community resilience and reduce vulnerability to future disasters by informing decision-making and guiding resource allocation through evidence-based insights on the effects of Cyclone Freddy on vegetation cover and resilience.

This study will establish a foundation for further research in this domain and contribute to the existing body of knowledge regarding the environmental impacts of cyclones. This study's documentation of Cyclone Freddy's effects on vegetation dynamics will significantly enhance future research on the resilience of natural ecosystems to extreme weather events. Future research aimed at understanding and mitigating the impacts of climate change on vegetation and ecosystems can leverage the methodologies developed and insights gained from this study.

CHAPTER 2: LITERATURE REVIEW

2.1 Tropical Cyclone Freddy in Malawi and its impact on Malawian communities.

According to Malawi government report (Government of Malawi, 2023), In March 2023, Malawi was severely affected by Tropical Cyclone Freddy. Following the heavy rains, multiple flood events and landslides were reported in Balaka, Blantyre, Chikwawa, Chiradzulu, Machinga, Mangochi, Mulanje, Mwanza, Neno, Nsanje, Ntcheu, Phalombe, Thyolo, and Zomba local authorities. More than 2,267,458 people were affected, including more than 659,278 displaced, with 679 deaths, 537 missing, and 2,186 injured. It is estimated that the among the total affected population, 1,308,064 are women and girls of reproductive age and about 100,297 of these are pregnant women. A great number of the fatalities following Tropical Cyclone Freddy were due to landslides in the Southern Highlands. This scenario differs from the impacts of similar recent cyclones, where flooding caused most of the fatalities.

According to report by Liston Mpheza, Cyclone Freddy was one of the deadliest and most destructive cyclones to have ever hit Malawi. It caused extensive damage to infrastructure, crops and homes, and resulted in the deaths of dozens of people from 17 to 27 March, 2023. It was one of the most devastating natural disasters to have ever hit the country.(Mpheza, 2023) The cyclone brought strong winds and torrential rains, leading to widespread flooding and destruction. More than 500 people were found dead and about 550 people were missing. The damage was estimated to be in the millions, with over 500,000 people affected and thousands of homes destroyed. Aid was sent from the international community to help the victims of the disaster. As the cyclone moved, it created strong winds, uprooting trees and destroying power lines and other infrastructure. The heavy rains caused flooding in many areas. and the unusually high tide meant that the flooding was even more severe than usual. The cost of the damage and the need for long-term aid drove the international community to respond with aid and support for the victims (Mpheza, 2023).

2.2 Areas within Blantyre that have been markedly influenced by Cyclone Freddy

Chilobwe in Blantyre, Malawi, was one of the most severely affected locations. The second-largest city in Malawi, Blantyre, suffered heavy losses, with hundreds more injured or reported missing in addition to the 190 verified deaths(Nabukulu et al., 2024). The community at large encountered tremendous difficulties while search and rescue efforts persisted in the middle of the persistent downpour. Similar degrees of devastation were also caused by mudslides and storm surges in the townships of Chemusa, Kabula, and, Ndirande and Mbayani(Issn, 2023)

2.3 Cyclone Freddy vs Vegetation and Land cover

Cyclone Freddy had a major negative impact on the ecosystem, especially on the amount of vegetation in areas like Blantyre, Malawi. Strong winds, copious amounts of rainfall, and consequent flooding are known to cause immediate and severe damage to vegetation during tropical storms like Freddy(Ding et al., 2024). It may take years for the land cover to recover from the deforestation, soil erosion, and other effects of these intense weather events(Akbar et al., 2019). The severe deforestation and soil degradation brought on by Cyclone Freddy, according to Braka et al. (Braka et al., 2024), emphasize the pressing need for efficient environmental monitoring and restoration initiatives in Malawi. According to studies, the immediate effects include uprooting trees, removing leaves, and destroying habitats, all of which significantly reduce biodiversity and ecological balance.

Moreover, cyclones compound the existing effects of land degradation, especially in regions already suffering from deforestation, unsustainable cultivation, and poor land management (Getahun, 2012). The removal of protective vegetation cover increases the susceptibility of land to erosion, landslides, and nutrient loss during extreme weather events (Ralisaona et al., 2023). In line with the biosphere-climate feedback theory, such changes in surface characteristics further influence local and regional climate by modifying surface albedo, evapotranspiration, and moisture recycling (Twabi et al., n.d.).

These findings are consistent with studies on ENSO-related climate variability, where years of climatic anomalies such as El Niño and La Niña episodes lead to observable shifts in vegetation dynamics and land cover patterns(Hoque, 2017). Thus, events like Cyclone Freddy represent not only isolated meteorological phenomena but also significant perturbations within the broader context of climate-vegetation interactions, necessitating detailed spatiotemporal monitoring for sustainable land and disaster management(Mpheza, 2023).

2.4 Factors Influencing Vegetation Resilience

Vegetation resilience is shaped by a complex interplay of climatic, topographic, and anthropogenic factors. Zhang et al. highlight that climatic variables such as precipitation, temperature, and vapor pressure deficit (VPD) are primary determinants of vegetation resilience(Ding et al., 2024). These factors influence growth recovery time and total growth reduction, with precipitation and temperature having significant impacts on regions such as Blantyre(Kadzuwa & Partnership, 2023). For instance, changes in precipitation and soil water availability can cause substantial spatial variability in resilience, as seen with the stronger effects in the Loess Plateau's high-growth recovery areas (X. Zhang et al., 2022). Furthermore, the interaction between climatic variables, such as the combination of radiant heat (SSR or temperature) and precipitation, nonlinearly enhances their individual effects, demonstrating the complexity of these interactions in influencing resilience (Ding et al., 2024).

2.5 Spatial Distribution of Vegetation Loss and Recovery in Areas

Cyclone Freddy had a significant effect on Blantyre's vegetation, especially in the vicinity of hills(Kadzuwa & Partnership, 2023). The complicated nature of ecological responses to such extreme climatic events is highlighted by the regional spread of vegetation loss and subsequent recovery. Hills and the areas around them frequently sustain more substantial damage as a result of the increased effects of water runoff and wind. There was a significant decrease in the amount of vegetation cover in the immediate aftermath of Cyclone Freddy due to widespread deforestation and soil erosion on the hillsides and other areas(Braka et al., 2024). According to research by

Chanza and Mafuta(Twabi et al., n.d.), the cyclone's intense rainfall triggered landslides and the uprooting of trees, which further increased the degree of vegetation loss on the steep slopes.

2.6 Remote Sensing in Disaster Assessment

Remote sensing and spatial analysis are efficient and accurate tools to provide useful information in every phase of cyclone disaster management(He et al., 2023). These tools support activities such as mapping, monitoring, and modelling of cyclone impacts to protect people, property, and the environment.

According to Hoque (Hoque, 2017), repeated high spatial resolution satellite imagery acquired before and after cyclone events significantly contributes to impact assessment and monitoring the progress of recovery. Object-based image analysis applied to moderate spatial resolution imagery, such as SPOT-5, was found to be effective for mapping the multiple impacts of cyclones, including vegetation defoliation, damage to cropland, destruction of settlements and infrastructure, and changes to landforms.

The approach achieved classification accuracies of 95.43% and 93.27% for pre- and post-cyclone images, respectively, and demonstrated the potential of remote sensing techniques to derive accurate and detailed spatial information at local scales, particularly in data-poor regions. These findings underscore the critical role of satellite remote sensing in cyclone disaster management and its ability to support informed planning and decision-making.

2.7 Spatial-Temporal Techniques in Cyclone Impact Assessment

Spatial-temporal techniques have become essential tools in assessing ecological impacts following disturbances such as cyclones. The integration of remote sensing and GIS allows for efficient monitoring of vegetation changes over large areas and long periods, offering high spatial and temporal resolution(Akhter & Hasan, 2025). Indicators such as the Normalized Difference Vegetation Index (NDVI) and Fractional Vegetation Cover (FVC) are widely used to analyze vegetation dynamics and the effects of climate variability and human activities. For instance, Zhang et al. (2022) employed multi-

temporal Landsat imagery from 1989 to 2021 in the Huainan mining area, applying regression slope analysis, correlation coefficients, and standard deviation ellipses to reveal vegetation trends(Z. Zhang et al., 2022). Their study showed a general decrease in vegetation cover, with significant spatial heterogeneity linked to both climatic and anthropogenic drivers. Such approaches are directly applicable in cyclone impact assessments, where understanding vegetation change patterns is key for effective ecological restoration planning.

2.8 Cyclone Freddy-Specific Studies in Malawi

Kadzuwa (2023) used Sentinel-2 imagery and NDVI analysis to assess vegetation damage, revealing significant losses in areas such as Nansato (NDVI: -0.5) and Nankuyu (-0.4), where deforestation and river proximity worsened flooding. Less affected areas (e.g., Bondo, NDVI: 0.3) were linked to higher elevations and better drainage. The study highlights NDVI's utility for rapid damage assessment and calls for targeted reforestation and flood mitigation. These findings align with broader research on geospatial tools for disaster response (Hu et al., 2017; Popa et al., 2019), emphasizing their role in prioritizing recovery efforts.

In the context of Cyclone Freddy, similar methodologies can be employed to assess the extent of environmental damage in Blantyre, Malawi. Kangoma et al. (2023) suggest that integrating remote sensing data with GIS mapping can offer a comprehensive view of the spatial distribution of vegetation changes, thereby informing effective restoration strategies.

2.9 Gaps in Current Research

There are still a lot of outstanding questions about the precise effects of Cyclone Freddy on the dynamics of the vegetation in Blantyre, despite a lot of research. Although earlier research has shed light on the overall effects of cyclones on vegetation, a closer examination is necessary due to the distinct environmental and socioeconomic circumstances of Blantyre. By using spatial and temporal analysis techniques to evaluate vegetation cover changes and resilience in the impacted areas, this research seeks to close these gaps.

CHAPTER 3: METHODOLOGY

3.1 Research Design

This study employs a quantitative research design to analyze the temporal and spatial dynamics of vegetation cover in areas affected by Cyclone Freddy within Blantyre, Malawi. The research is grounded in the use of remote sensing and geographic information system (GIS) technologies, which enable systematic, data-driven assessment of vegetation change over time(Ding et al., 2024). The study specifically focuses on four urban neighborhoods: Ndirande, Chilomoni, Nyambadwe, and Soche-Chilobwe.

High-resolution Sentinel-2 imagery was used to generate Normalized Difference Vegetation Index (NDVI) values for two time periods: October 2022 (pre-cyclone) and October 2023 (post-cyclone). Through this approach, changes in vegetation cover were quantitatively assessed using NDVI differencing and spatial analysis. These methods provided insight into both the magnitude and distribution of vegetation disturbance and recovery following the cyclone event.

Potential confounding variables such as land use changes and anthropogenic activities—which may independently influence vegetation dynamics—were acknowledged as factors that could affect the accuracy of the findings. Efforts were made to account for these influences during analysis and interpretation.

In this study, the occurrence of Cyclone Freddy is treated as the independent variable, while the temporal-spatial variation in vegetation cover constitutes the dependent variable. Operational definitions of vegetation cover include NDVI-derived indicators such as vegetation density, coverage extent, and vegetation health status.

The primary goal of this research is to contribute to a deeper understanding of vegetation resilience in cyclone-affected urban landscapes. The findings are intended to support improved disaster preparedness, environmental monitoring, and urban resilience planning in Malawi and similarly vulnerable regions. Figure 4 present the workflow that was followed when doing the research

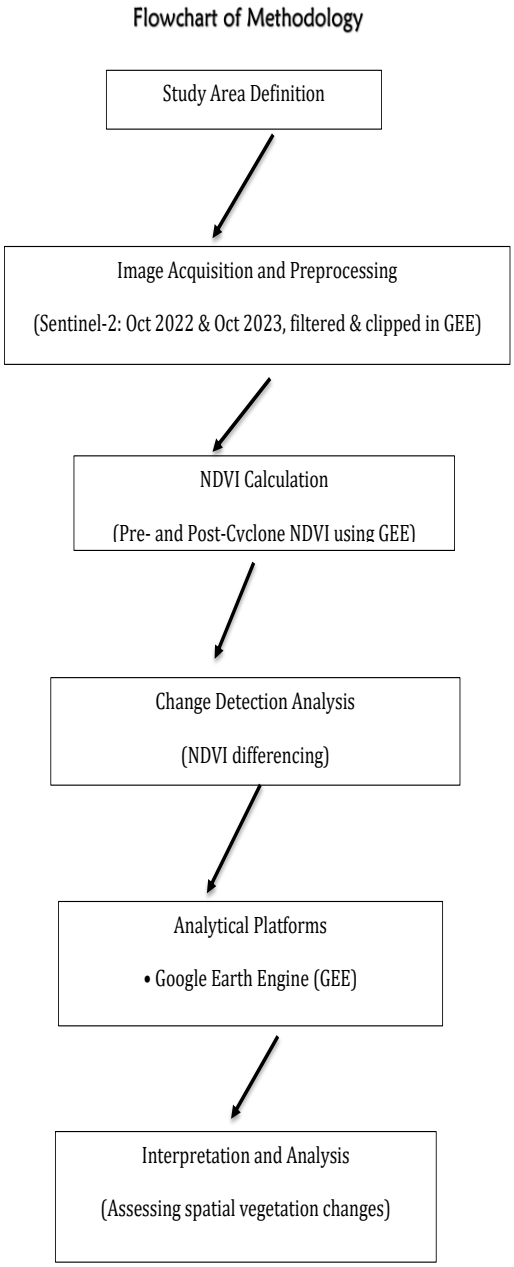


Figure 3: Methodology flowchart followed during research.

3.2 Materials and methods

3.2.1 Study Area:

The southern part of Malawi, specifically Blantyre, is the subject of the study. Located roughly 250 kilometers south of Lilongwe, the capital(Bagcchi, 2022). Blantyre is a significant industrial and commercial center. Cyclone Freddy had a major impact on the

area, changing the vegetation cover and posing serious environmental and socioeconomic problems(Mpheza, 2023).Within Blantyre, the research specifically concentrates on four high-density and topographically diverse communities: Ndirande, Chilomoni, Nyambadwe, and Soche-Chilobwe.

3.2.1.1 Chilobwe_Soche:

This area experienced devastating mudslides that resulted in a high number of fatalities. For instance, ten members of one family from Chilobwe Zambezi Evangelical Church were swept away by flash flooding. Search and rescue teams recovered a significant number of bodies in Soche, indicating the severity of the impact in this area. The area under Mount Soche experienced significant devastation from flash flooding and mudslides.(Twabi et al., n.d.)(Baresford, 2023)

3.2.1.2 Ndirande:

Areas near Ndirande hills were also heavily affected, with houses being completely washed away and many deaths reported.(Baresford, 2023)(Mlanjira, 2023)

3.2.1.3 Chilomoni:

Areas near these Chilomoni mountains were also heavily affected, with houses being completely washed away and many deaths reported. (Baresford, 2023)

3.2.1.4 Nyambadwe:

This area experienced devastating mudslides that resulted in a high number of fatalities.(Kabukuru & Gondwe, 2023)

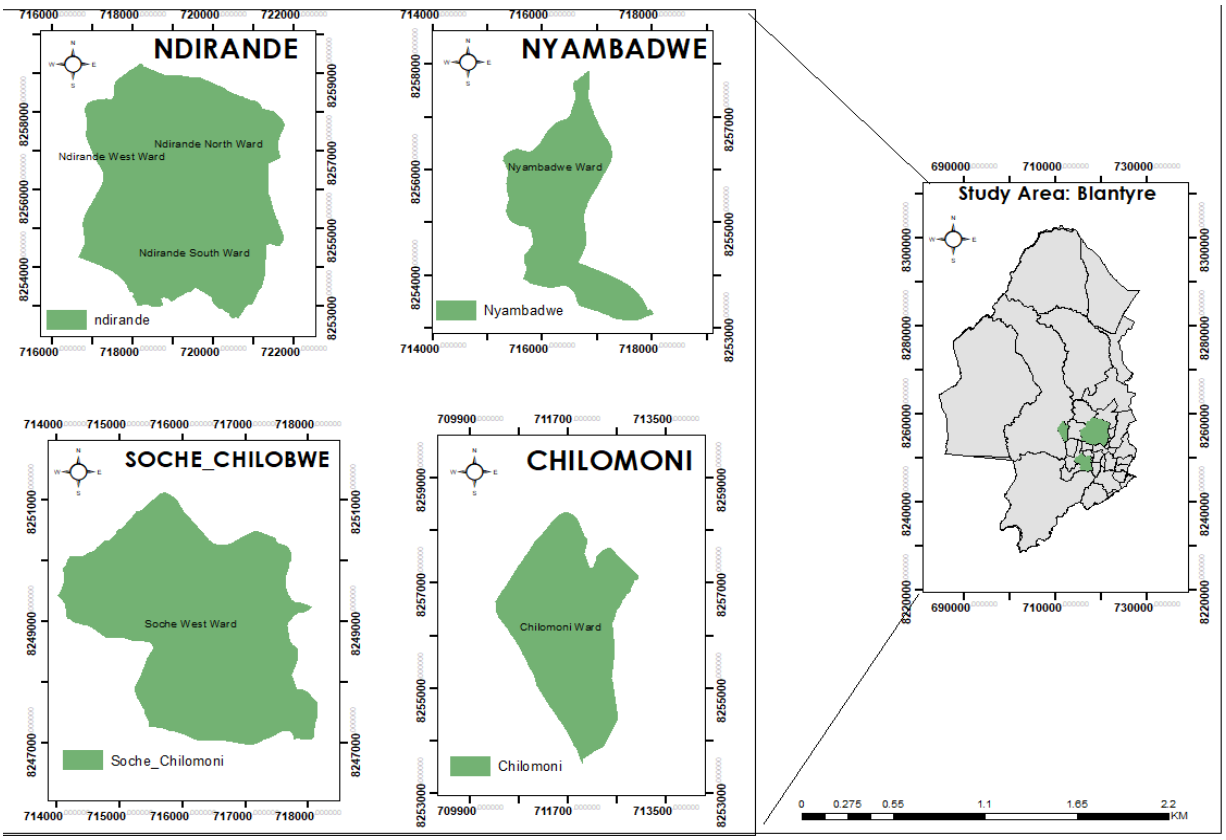


Figure 4: Map of Blantyre depicting areas of Focus: Ndirande, Nyambadwe, Soche_Chilobwe and Chilomoni

3.2.2 Earth Observations Data:

3.2.2.1 Data Sources and Collection

In this study, a combination of geospatial tools was used to collect, process, and analyze satellite imagery and spatial data. The main software platforms included Google Earth Engine (GEE), ArcMap, and QGIS. Sentinel-2 imagery was accessed through GEE (ee.ImageCollection("COPERNICUS/S2_HARMONIZED")) to create cloud-free median composites for October 2022 and October 2023, representing conditions before and after Cyclone Freddy.

The focus was on four areas in Blantyre —Ndirande, Chilomoni, Nyambadwe, and Soche-Chilobwe—which were among the areas most affected by the cyclone. Choosing October for both years helped ensure consistency in seasonal conditions, making it easier to detect real changes in vegetation cover without interference from seasonal variation

3.2.2.2 Satellite Data Acquisition Summary

Summary of data collected for before cyclone assessment

Table 1: Before Cyclone Freddy (October 2022)

Area	Satellite	Sensor	Bands	Date of Acquisition	Spatial Resolution	Cloud Cover (%)	Source
Chilobwe	Sentinel-2	MSI	B2–B8, B11, B12	2022/10/01-2022/10/30	10m	<10%	(GEE)
Ndirande	Sentinel-2	MSI	B2–B8, B11, B12	2022/10/01-2022/10/30	10m	<10%	(GEE)
Chilomoni	Sentinel-2	MSI	B2–B8, B11, B12	2022/10/01-2022/10/30	10m	<10%	(GEE)
Soche-Chilobwe	Sentinel-2	MSI	B2–B8, B11, B12	2022/10/01 to 2022/10/30	10m	<10%	(GEE)

Table 2 : After Cyclone Freddy (October 2023)

Area	Satellite	Sensor	Bands	Date of Acquisition	Spatial Resolution	Cloud Cover (%)	Source
Chilobwe	Sentinel-2	MSI	B2–B8, B11, B12	2023/10/01-2023/10/30	10m	<10%	(GEE)
Ndirande	Sentinel-2	MSI	B2–B8, B11, B12	2023/10/01-2023/10/30	10m	<10%	(GEE)
Chilomoni	Sentinel-2	MSI	B2–B8, B11, B12	2023/10/01-2023/10/30	10m	<10%	(GEE)
Soche-Chilobwe	Sentinel-2	MSI	B2–B8, B11, B12	2023/10/01-2023/10/30	10m	<10%	(GEE)

Despite the Sentinel-2 satellite imagery datasets being unrestricted (free and open)(Vrieling et al., 2019), their preference was largely due to the following;

The capability of the mission's imaging sensors' red-edge (RE) of the Near InfraRed (NIR) window that is used to detect vegetation at moderate spectral resolution of 10-20m(Yan et al., 2018). Such a scale provides fine details of observations, and

The assessment of the vegetation damage/change that uses the Normalized Difference Vegetation Index (NDVI) technique (Vrieling et al., 2019).This is rendered possible by being provided the Near-Infrared (NIR) Red-Edge spectral region of the Sentinel-2 MSI imagery. The NIR is located in the sharp change of canopy reflectance range between 680nm and 750nm where a slope occurs, providing an advantage to mapping vegetation(Lacroix et al., 2018). The satellite data acquisition parameters used in this study are summarized in Appendix C.

3.3.3.1 Normalized Difference Vegetation Index (NDVI)

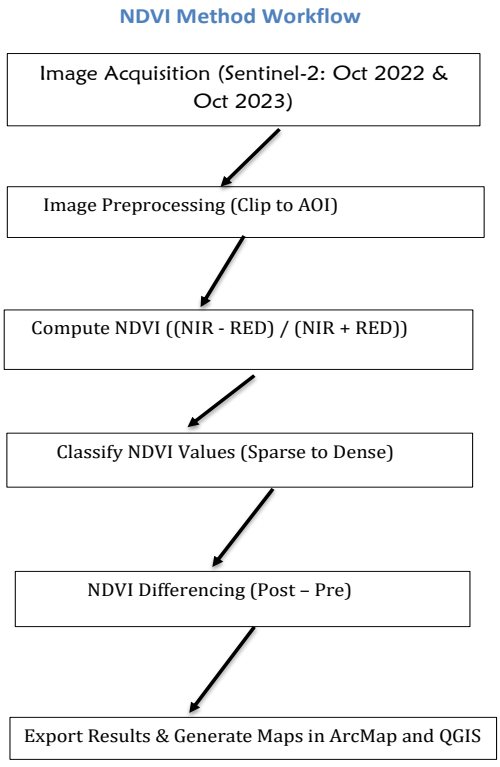


Figure 5: Workflow of NDVI method.

The term Normalized Difference Vegetation Index (NDVI) simply refers to a graphical indicator most widely characterized in plant studies, and it is correlated with green leaf cover, and consequently biomass set by the plant physiology i.e., when canopy cover is correlated with biomass(Vrieling et al., 2019). NDVI is particularly useful in detecting vegetation stress, health, and cover changes—making it suitable for post-disaster environmental assessments(Hoque, 2017).

It is simply calculated as follows(Yan et al., 2018);

Equation 1: NDVI formula

$$\text{NDVI} = \frac{NIR - RED}{NIR + RED}$$

Where;

- NDVI = Normalized Difference Vegetation Index
- NIR = Near-Infrared band of the Electromagnetic Spectrum (EMS), and
- Red = the optical (visible) red band of the EMS.

NDVI interpretation is based on the simple principle that healthy vegetation (chlorophyll) reflects more Near-InfraRed (NIR) and green light compared to other wavelengths. In contrast, it absorbs more red and blue light(Vrieling et al., 2019)(Yan et al., 2018). The general trend is that NDVI values range from -1.0 to 1.0, and the negative values indicate clouds and water, while the positive ones near zero indicate bare soil(Akhter & Hasan, 2025).

Table 3: Classification schema for vegetation cover. (Shabab et al., 2025)(Hoque, 2017)

Type of vegetation	NDVI value intensity
Water or No vegetation	(−)1 - (−)0.03
Slightly dense	(−)0.03 - 0.25
Moderately dense	0.26 - 0.35
Highly dense	0.36 - 1

Therefore, in this research, the higher positive range of values for NDVI, i.e., 0.1 to 0.5 denote the transition from bare land/dead or sparse vegetation to dense green vegetation (≥0.6). In this case, the higher positive values would signify the areas where the cyclone affected less while the low ones denote those were highly affected. Details of the GEE code scripts for NDVI calculations and data exportation are provided in Appendix A.

The NDVI numerical difference was computed by getting the change (after subtracting the before disaster scene covering 01-10-2022 to 30-10-2022 from the post-disaster scenes covering 01-10-2023 to 30-10-2023), thus (post-pre).

Equation 2: Change detection formula

$$\Delta NDVI = NDVI_{2023} - NDVI_{2022}$$

The raster calculator expression used for NDVI change detection analysis is outlined in Appendix B.

3.3.4 Sentinel-2 Imagery Processing

1. The key Sentinel-2 Imagery processing tasks involved the following
2. Selection of Area of Interest – Nyambadwe, Ndirande, Chilomoni and Soche_Chilobwe
3. Selection of time periods, 01-10-2022 to 30-10-2022 as pre disaster and 01-10-2023 to 30-10-2023 as post disaster.
4. Masking out of clouds- done to reduce the radiometric distortion of land surfaces of the AOIs and also to remove dark pixels due to the effect of cloud shadows. The maximum cloud cover was 10%.
5. Selection of theme category and appropriate technique i.e., Vegetation and NDVI
6. Calculation of AOI scenes difference (Post cyclone minus Before cyclone) and generation of results.

The outputs from GEE were subsequently exported for further spatial analysis and map production using ArcMap and QGIS. These platforms were used to refine cartographic outputs and to integrate vector datasets for enhanced interpretation of vegetation change across the selected AOIs.

CHAPTER 4: RESULTS AND DISCUSSION

This section presents the findings of the vegetation change assessment based on the one core analytical method applied in this study: Normalized Difference Vegetation Index (NDVI) analysis.

4.1 Temporal NDVI Changes for AOI Within Blantyre

4.1.1 NYAMBADWE

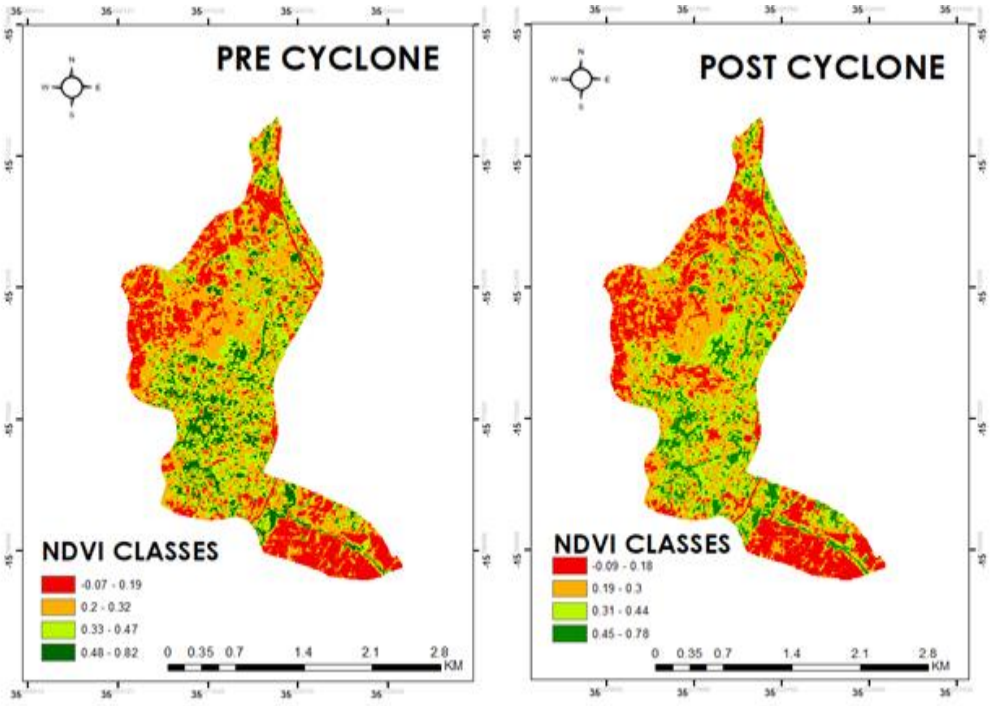


Figure 6: NDVI map for Nyambadwe depicting for both pre and post periods

Before Cyclone Freddy, Nyambadwe exhibited a heterogeneous vegetation landscape, with NDVI values ranging from -0.07 to 0.82. Much of the neighborhood was characterized by slightly to moderately dense vegetation, particularly around residential and semi-developed areas, while healthier and denser vegetation patches (NDVI > 0.36) were mainly concentrated along open spaces, vegetated slopes, and ridges. After the cyclone, NDVI values shifted downward to a range of -0.09 to 0.78, reflecting a general decline in vegetation health. Significant reductions were noted particularly in low-lying areas, although patches of moderately to highly dense vegetation persisted in upland zones, suggesting localized resilience. (See figure 7)

The spatial variability in vegetation change aligns with findings by Akbar et al. (Akbar et al., 2019), who emphasized the role of topography in influencing vegetation density within urban environments. The moderate pre-cyclone vegetation stress observed can be attributed to urban settlement expansion, as similarly discussed by Shabab et al. (Shabab et al., 2025). Post-cyclone vegetation degradation, particularly in flood-prone areas, supports observations by Vrieling et al. (2019), who reported that cyclone-induced impacts, such as defoliation and flooding, contribute significantly to vegetation stress in urban and peri-urban landscapes.

4.1.1.1 Change Detection Analysis – NDVI Differencing

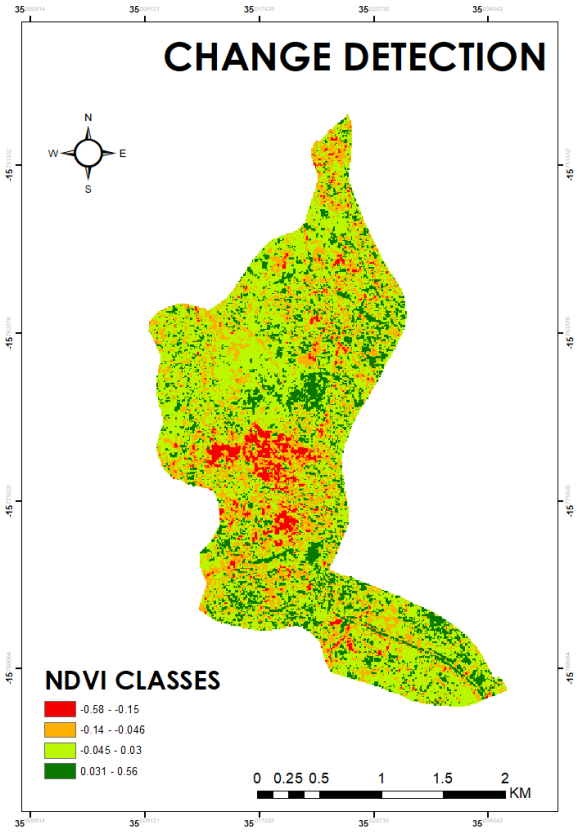


Figure 7: Change detection Map for Nyambadwe

The change detection analysis for Nyambadwe (see Figure 8) highlights the spatial variations in vegetation dynamics post-cyclone. NDVI differences ranged from approximately -0.58 to 0.56, indicating that certain areas experienced significant vegetation loss while others showed signs of recovery. The central and northern parts of Nyambadwe recorded the highest negative NDVI changes, reflecting substantial degradation, whereas patches of positive change were observed in isolated upland zones.

The NDVI-based change detection analysis in this study aligns with established methods for assessing cyclone-induced vegetation damage, as seen in Vrieling et al. (Vrieling et al., 2019) and Hoque (2017). The negative NDVI differences, reflecting vegetation loss, match findings by Joyce et al. (Ding et al., 2024), who linked this damage to defoliation and erosion. Positive NDVI differences, indicating recovery, support Akhter & Hasan (Akhter & Hasan, 2025), who found that resilience is influenced by topography and vulnerability. This study contributes to the growing literature on how vegetation responds to cyclones, especially in urban and peri-urban areas, where both natural and human factors play a role in resilience.

4.1.2 CHILOMONI

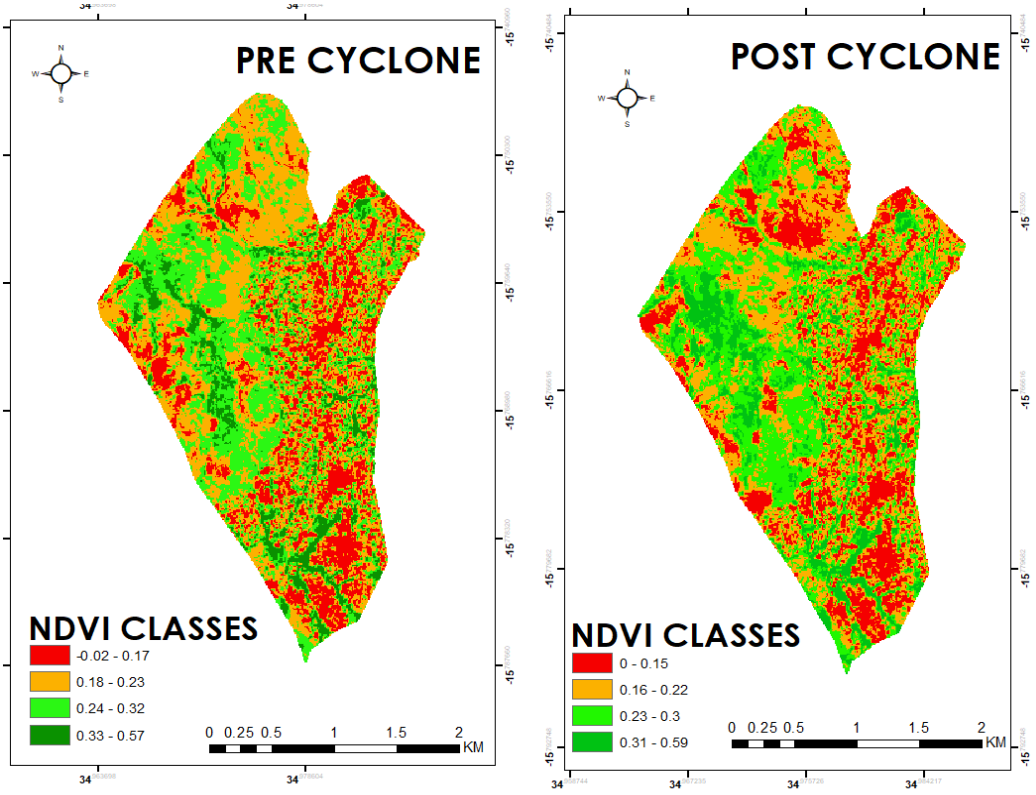


Figure 8: NDVI map for Chilomoni depicting for both pre and post periods

The pre- and post-cyclone NDVI variations observed in Chilomoni (see figure 9), indicating a general decline in vegetation health, align with findings by Ding et al. (2024) and Braka et al. (2024), who emphasized the destructive role of tropical cyclones through mechanisms such as canopy loss, uprooting, and soil erosion.

Studies like Hoque (2017) have shown that moderate NDVI reductions post-cyclone often reflect a combination of immediate vegetation stress and longer-term degradation processes. Furthermore, as noted by Akbar et al. (2019), post-disaster vegetation recovery can be spatially uneven, influenced by pre-existing land use patterns, soil conditions, and topography. These dynamics are evident in Chilomoni, where some patches retained relatively healthier vegetation while others showed pronounced degradation, demonstrating the heterogeneous impact typical of cyclone-affected urban landscapes.

4.1.2.1 Change Detection Analysis – NDVI Differencing

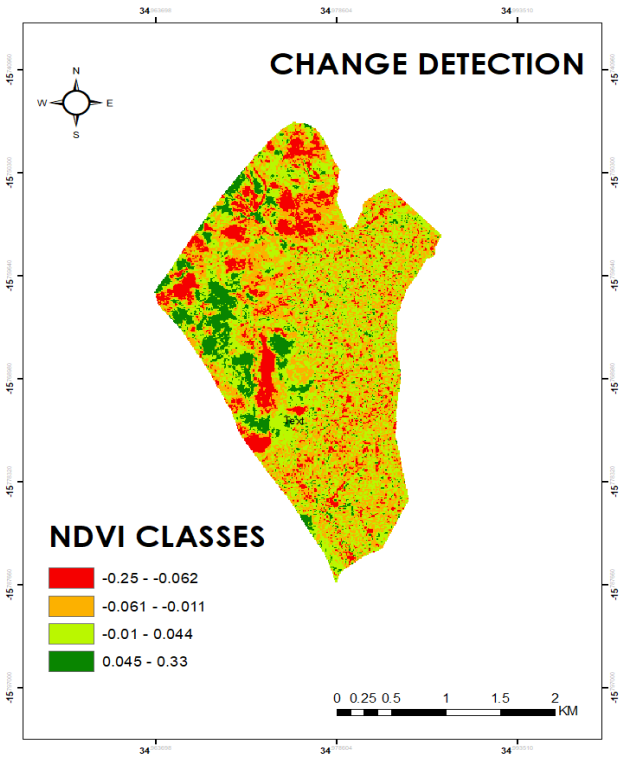


Figure 9: Change detection map for Chilomoni

The NDVI change detection results for Chilomoni, showing a mix of severe vegetation loss and localized recovery, align with findings by Mpheza (2022), who emphasized that urban and peri-urban environments in Malawi are highly susceptible to vegetation degradation due to poor land management and extreme weather exposure.

The severe loss zones, corresponding to negative NDVI differences, reflect patterns observed by Shibuya et al. (2024), where tropical storms caused widespread canopy removal and soil destabilization. Conversely, the areas demonstrating resilience and regrowth, particularly in upland regions, support observations by Kadzuwa and Maonga (2015), who noted that topography and drainage patterns play critical roles in post-disaster vegetation recovery. These results reinforce the complexity of cyclone impacts on urban vegetation, shaped by both environmental and anthropogenic factors.

4.1.3 Soche and Chilobwe regions

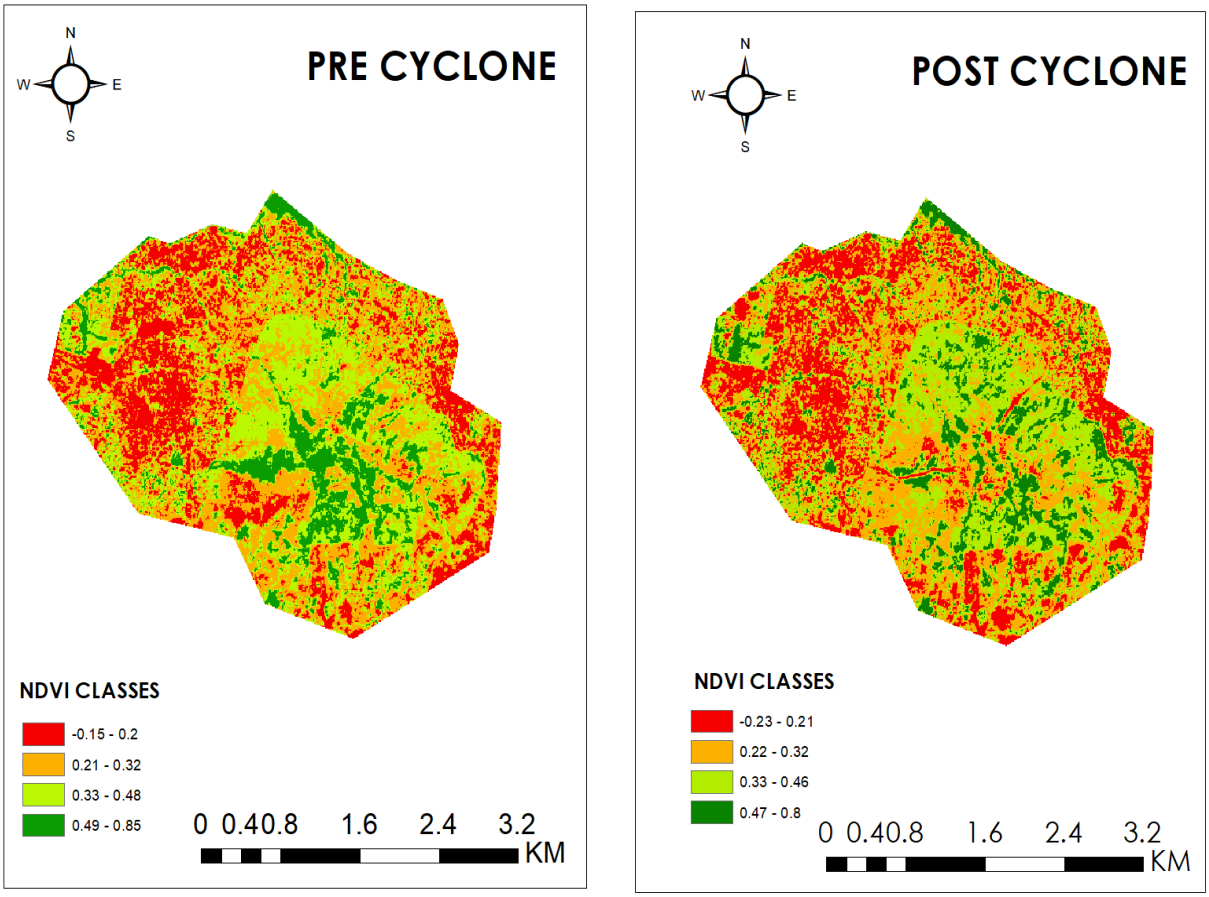


Figure 10: NDVI map for Soche_Chilobwe depicting for both pre and post periods

Before Cyclone Freddy, Chilobwe-Soche exhibited diverse vegetation health, with NDVI values ranging from 0.15 to 0.85, indicating a mixture of sparse, moderately healthy, and dense vegetation. These findings align with Akhter & Hasan (2025), who highlighted that urban areas typically show lower NDVI values due to human activities and land

degradation. Following the cyclone, NDVI values in Chilobwe ranged from 0.21 to 0.80, suggesting a general decline in vegetation health but with significant areas of recovery.

The most affected regions, showing NDVI values between 0.21–0.22, likely experienced defoliation and vegetation stress, consistent with Vrieling et al. (2019), who documented significant vegetation damage in low-lying, flood-prone areas. However, areas with NDVI values between 0.33–0.46 demonstrated moderate recovery, indicating resilience, particularly in elevated zones that had better drainage.

This supports the observations by Shabab et al. (2025), who noted that topographical features play a crucial role in post-cyclone vegetation dynamics. The persistence of vegetation in the 0.47–0.80 range further suggests resilience, which aligns with Joyce et al. (2009), who found that areas less exposed to extreme weather conditions tend to exhibit more rapid vegetation recovery.

4.1.3.1 Change Detection Analysis – NDVI Differencing

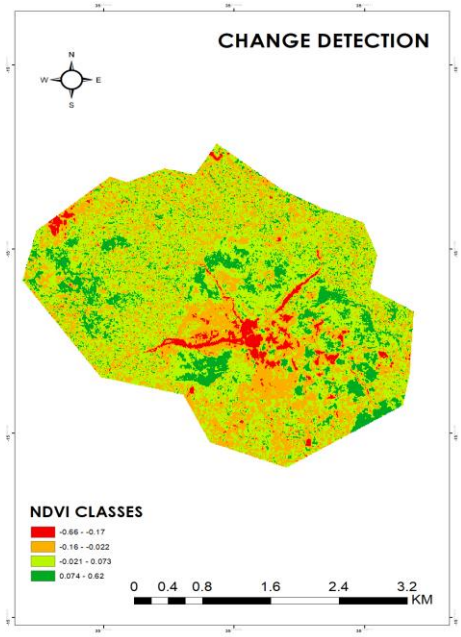


Figure 11: Change detection Map for Soche_Chilobwe

The NDVI change detection results for Soche and Chilobwe revealed both vegetation loss and recovery after Cyclone Freddy. Areas with NDVI differences between -0.66 and 0.17 experienced notable degradation, particularly in exposed and mudslide-prone zones,

consistent with Braka et al. (2024), who linked such damage to topographical vulnerability. Positive NDVI changes between 0.074 and 0.62 highlighted zones of resilience, particularly in upland areas, supporting findings by Hoque (Hoque, 2017). Overall, the spatial variability observed aligns with Mpheza (2022), who emphasized that urban land cover and elevation strongly influence post-cyclone vegetation impacts.

4.1.4 NDIRANDE

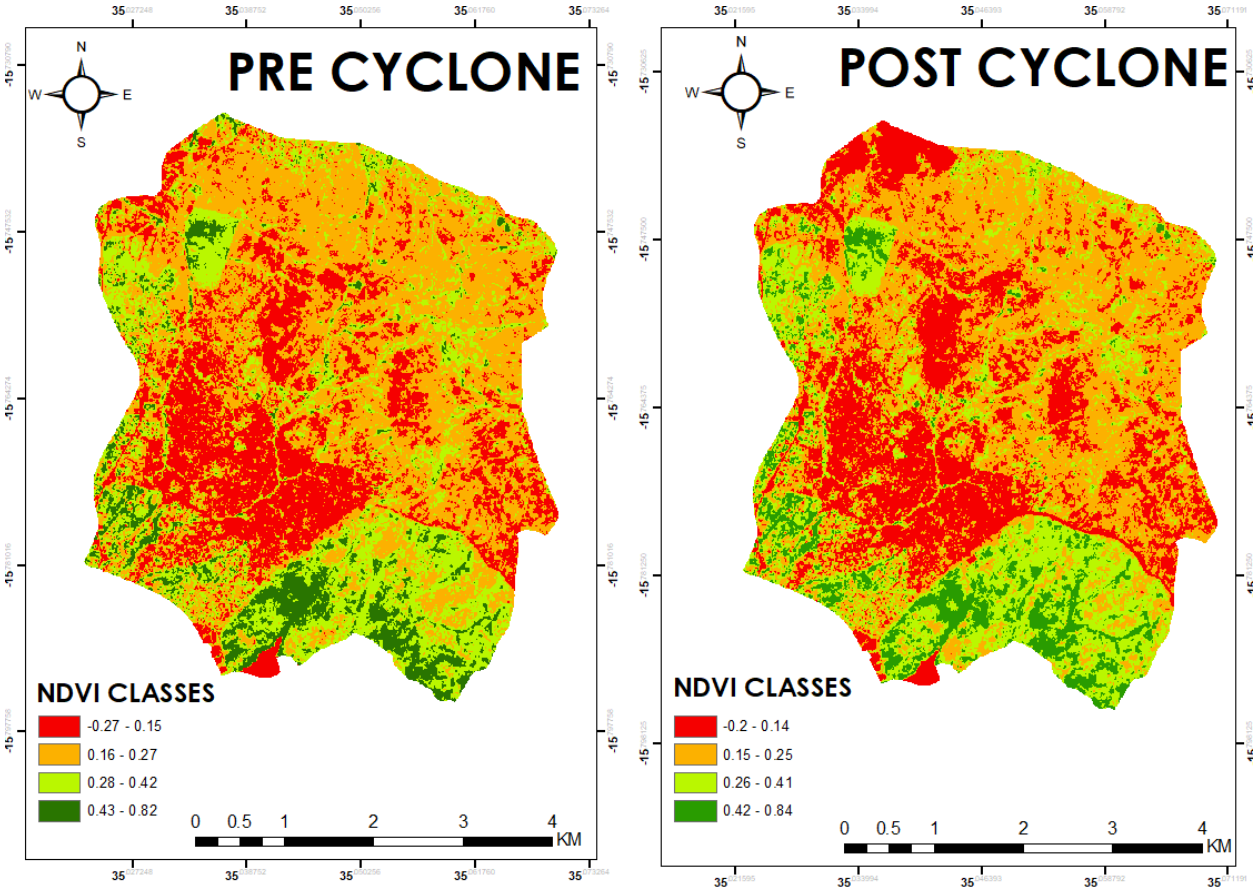


Figure 12: NDVI map for Ndirande depicting for both pre and post periods

In Soche and Chilobwe, the NDVI change detection analysis revealed significant variation in vegetation response to Cyclone Freddy. Areas with NDVI differences ranging from -0.66 to 0.17 indicated substantial vegetation degradation, particularly in exposed or mudslide-prone zones, consistent with findings by Vrieling et al. (2019), who noted that low-lying or unstable areas are particularly vulnerable to extreme weather events.

On the other hand, areas with NDVI values between -0.16 and 0.073 showed partial vegetation loss but with signs of recovery, supporting the observations of Shabab et al. (2025), who highlighted that urban landscapes can show mixed patterns of recovery due to topography and land use. Furthermore, the positive NDVI changes between 0.074 and 0.62, suggesting resilient or regenerating vegetation, particularly in upland areas, align with Akhter & Hasan (2025), who pointed out that well-drained and elevated regions tend to exhibit quicker recovery after cyclonic events. These results emphasize the heterogeneous nature of cyclone impacts, with recovery occurring more rapidly in areas with favorable topographical conditions

4.1.4.1 Change Detection Analysis – NDVI Differencing

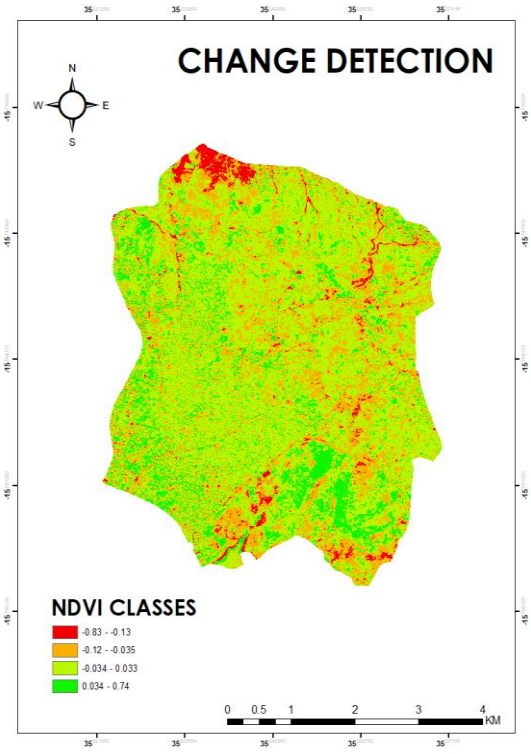


Figure 13: Change detection Map for Ndirande

The NDVI change detection analysis for Ndirande showed severe vegetation degradation between –0.83 and –0.13, mainly in low-lying, densely populated areas. Moderate disturbance was observed between –0.12 and –0.035, while zones with NDVI changes from –0.034 to 0.033 indicated partial persistence. Positive NDVI changes between 0.034 and 0.74 reflected vegetation resilience and regrowth, particularly in upland sections.

These patterns align with findings by Mpheza (2022) and Kadzuwa (Kadzuwa & Partnership, 2023) which both highlighted the role of urban density and topography in influencing post-cyclone vegetation dynamics

.

Table 4: Summary of NDVI Results for Study Areas

Study Area	Pre-Cyclone NDVI Range	Post-Cyclone NDVI Range	Observations (Pre-Cyclone)	Observation (post-cyclone)
Nyambadwe	-0.07 to 0.82	-0.09 to 0.78	Healthy vegetation in many parts; some sparse zones	General decline in vegetation health, localized recovery
Chilomoni	0.02 to 0.57	0.15 to 0.50	Moderately healthy to dense vegetation, some stressed zones	Noticeable vegetation loss but signs of regrowth in parts
Soche& Chilobwe	0.15 to 0.85	0.21 to 0.80	Very healthy vegetation, especially in mature areas	Moderate reduction; some patches resilient and recovering
Ndirande	-0.27 to 0.82	-0.20 to 0.84	Ecologically diverse: dense vegetation patches amid urban zones	Significant vegetation loss in urban lowlands; resilience patches on uplands

Table 5:Summary of Change Detection Analysis for Study Areas

Study Area	NDVI Change Range	Major Observations (Change Detection)	Overall Interpretation
Nyambadwe	-0.58 to 0.56	Severe vegetation loss in low NDVI zones; localized regrowth in higher NDVI classes	Mixed impact: significant loss with patches of resilience
Chilomoni	-0.25 to 0.33	Localized severe vegetation degradation with moderate recovery zones	Partial recovery visible; heterogeneous impact
Soche & Chilobwe	-0.66 to 0.62	Vegetation damage in lower NDVI zones; strong regrowth in upland areas	Evidence of both vegetation loss and early recovery
Ndirande	-0.83 to 0.74	Extensive vegetation loss across urban zones; strong resilience in some upland areas	Severe impact but clear patches of regrowth

CHAPTER 5: CONCLUSIONS AND RECOMMENDATIONS

5.1 Conclusion

Results from the NDVI approach indicated significant vegetation loss across the study areas, particularly in Ndirande and Chilomoni, where declines in NDVI values were observed. Nyambadwe also experienced vegetation degradation, although some sections demonstrated partial resilience and early recover. Areas such as Soche-Chilobwe demonstrated vegetation resilience and early signs of regrowth. Pre-cyclone NDVI values ranged widely from –0.27 to 0.85, reflecting diverse and relatively healthy vegetation cover, whereas post-cyclone values exhibited a general downward shift, indicating disturbance and stress. Change detection analysis confirmed the spatial variability of Cyclone Freddy's impact, with low-lying areas showing more severe damage than elevated zones.

By comparing pre- and post-cyclone NDVI imagery, the study successfully identified areas most vulnerable to environmental degradation, providing essential insights for disaster response planning and resilience-building efforts. The outputs generated from the NDVI analysis serve as a valuable resource for decision-makers and urban planners in understanding cyclone impacts and prioritizing recovery strategies. Ultimately, this study supports efforts by agencies such as DoDMA in making informed, evidence-based decisions for post-cyclone recovery, while demonstrating the critical role of geospatial analysis in disaster management.

While this study successfully applied NDVI analysis to assess vegetation changes following Cyclone Freddy in Blantyre, several limitations must be highlighted. The absence of ground-truth validation data limited the ability to confirm the accuracy of NDVI interpretations. The analysis focused solely on vegetation cover changes without integrating anthropogenic factors (such as land use practices, urbanization) or biophysical factors (such as soil type, topography, or drainage), which also significantly influence vegetation dynamics. Future research incorporating these variables would provide more understanding of disaster impacts.

5.2 Recommendations

Based on the findings of this study, it is also recommended that local authorities and disaster management agencies prioritize vegetation restoration programs in heavily degraded areas such as Ndirande and Chilomoni. Integrating remote sensing monitoring systems into urban planning and disaster risk management frameworks would support real-time tracking of environmental changes. Additionally, the establishment of urban greening initiatives and the protection of natural buffers like forests and wetlands should be promoted to enhance ecological resilience against future extreme weather events. Capacity-building programs in geospatial technologies should also be encouraged to strengthen local technical expertise in post-disaster environmental assessments.

Future research should conduct ground-truth validation which would enhance the accuracy and reliability of remote sensing interpretations. To achieve a more holistic understanding of cyclone impacts, future studies should also consider analyzing anthropogenic factors (e.g., settlement patterns, agricultural practices) and biophysical factors (e.g., soil properties, slope, hydrology), which may influence vegetation resilience and degradation. Expanding the geographic scope to include broader regions affected by Cyclone Freddy could further improve disaster preparedness and environmental recovery strategies.

CHAPTER 6: REFERENCES

Akbar, T. A., Hassan, Q. K., Ishaq, S., Batool, M., Butt, H. J., & Jabbar, H. (2019). Investigative spatial distribution and modelling of existing and future urban land changes and its impact on urbanization and economy. *Remote Sensing*, *11*(2). https://doi.org/10.3390/rs11020105

Akhter, J., & Hasan, G. M. J. (2025). Mapping vegetation change and cyclonic effects along the coastal regions of Bangladesh: A spatio-temporal perspective. *Regional Studies in Marine Science*, *81*(November 2024), 103924. https://doi.org/10.1016/j.rsma.2024.103924

Bagcchi, S. (2022). Malawi takes on cholera outbreak amid cyclone devastation. *The Lancet Microbe*, *3*(7), e480. https://doi.org/10.1016/s2666-5247(22)00131-8

Baresford, M. (2023, March 15). *Cyclone Freddy and its tragic consequences – Zambesi Mission*. https://zambesimission.org/cyclone-freddy-and-its-tragic-consequences/

Braka, F., Daniel, E. O., Okeibunor, J., Rusibamayila, N. K., Conteh, I. N., Yur, C. T., Patrick, O., Ramadan, C., Byakika-, J., Ochien, E. M., Kagoli, M., & Chauma-, A. (2024). *Effects of tropical cyclone Freddy on the social determinants of health : the narrative review of the experience in Malawi*. 1–10. https://doi.org/10.1136/bmjph-2023-000512

Ding, Y., Feng, Y., Chen, K., & Zhang, X. (2024). Analysis of spatial and temporal changes in vegetation cover and its drivers in the Aksu River Basin, China. *Scientific Reports*, *14*(1), 1–16. https://doi.org/10.1038/s41598-024-60575-9

Getahun, Y. S. (2012). *Spatial-temporal analysis of climate elements, vegetation characteristics, and sea surface temperature anomaly – a case study in Gojam, Ethiopia*.

Government of Malawi. (2023). *Malawi 2023 Tropical Cyclone Freddy Post-Disaster Needs Assessment*. *April*, 1–102. https://www.preventionweb.net/media/87994/download?startDownload=true

He, Z., Yue, T., Chen, Y., Mu, W., Xi, M., & Qin, F. (2023). Analysis of Spatial and Temporal Changes in Vegetation Cover and Driving Forces in the Yan River Basin, Loess Plateau. *Remote Sensing*, *15*(17). https://doi.org/10.3390/rs15174240

Hoque, M. A.-A. (2017). *Cyclone disaster mapping, monitoring and management using satellite remote sensing and spatial analysis*. 160. http://espace.library.uq.edu.au/view/UQ:685421

Issn, O. (2023). *African Journal of Primary Health Care & Family Medicine Cyclone Freddy in Malawi : Reflections from a primary care perspective*. 3–6.

Kabukuru, W., & Gondwe, G.-V. (2023, March 17). *Locals pick up pieces after Cyclone Freddy as death toll rises | PBS News*. https://www.pbs.org/newshour/world/locals-pick-up-pieces-after-cyclone-freddy-as-death-toll-rises

Kadzuwa, H., & Partnership, S. M. (2023). *POST CYCLONE FREDDY DISASTER MAPPING-MALAWI A report prepared by*. *August*.

Lacroix, P., Bièvre, G., Pathier, E., Kniess, U., & Jongmans, D. (2018). Remote Sensing of Environment Use of Sentinel-2 images for the detection of precursory motions before landslide failures. *Remote Sensing of Environment*, *215*(March), 507–516. https://doi.org/10.1016/j.rse.2018.03.042

Mlanjira, D. (2023, March 14). *Malawi Police Recover Over 100 Dead Bodies in Blantyre and Surrounding Areas - allAfrica.com*. https://allafrica.com/stories/202303140230.html

Mpheza, L. (2023). The Impact of Cyclone Freddy on Malawian Communities: Examining Truth, Resilience, Hope, Recovery for Victims and Recommendations. *International Journal of Innovative Science and Research Technology*, *8*(3), 2185–2192. www.ijisrt.com

Nabukulu, C., Jetten, V. G., & Ettema, J. (2024). Implications of Tropical Cyclone Rainfall Spatial–Temporal Variability on Flood Hazard Assessments in the Caribbean Lesser Antilles. *GeoHazards*, *5*(4), 1275–1293. https://doi.org/10.3390/geohazards5040060

Ralisaona, F., Randimbiarison, J. R., Mauluka, C., & Konate, B. (2023). Supporting Preparedness and Response to Cyclone Freddy In Madagascar- A Contribution from the Social and Behaviour Change Communication. *Archives of Health Science*, *November*, 1–14. https://doi.org/10.31829/10.31829/2641-7456/ahs2023-7(1)-028

Shabab, K. J., Shahed, M. H., & Malek, M. B. (2025). *Spatio-Temporal Analysis of Vegetation Cover in Char Fasson and Galachipa Upazila of Bangladesh (1994-2024) Using Landsat Imagery*. *17*(1), 66–79. https://doi.org/10.4236/jgis.2025.171004

Twabi, H. H., Jafali, J., Mndala, L., Riches, J., Monk, E. J. M., Phiri, D., Makuluni, R., Gadama, L., Kachale, F., Bilesi, R., Mbewe, M., Likaka, A., Chapuma, C., Kumwenda, M., Maseko, B., Ndamala, C., Kuyere, A., Munthali, L., Henrion, M. Y. R., … Twabi, H. (n.d.). *Cyclone Freddy and its Impact on Women's Health: Data from a National Maternal Surveillance Platform in Malawi Contributing authors*. https://ssrn.com/abstract=4696502

Vrieling, A., Meroni, M., Darvishzadeh, R., Skidmore, A. K., Wang, T., Zurita-milla, R., Oosterbeek, K., Connor, B. O., & Paganini, M. (2019). Remote Sensing of Environment Vegetation phenology from Sentinel-2 and fi eld cameras for a Dutch barrier island. *Remote Sensing of Environment*, *215*(March 2018), 517–529. https://doi.org/10.1016/j.rse.2018.03.014

Yan, L., Roy, D. P., Li, Z., Zhang, H. K., & Huang, H. (2018). *Remote Sensing of Environment Sentinel-2A multi-temporal misregistration characterization and an orbit- based sub-pixel registration methodology*. *215*(September 2017), 495–506. https://doi.org/10.1016/j.rse.2018.04.021

Zhang, X., Liu, Y., Chen, X., Long, L., Su, Y., Yu, X., Zhang, H., Chen, Y., & An, S. (2022). Analysis of spatial and temporal changes of vegetation cover and its driving forces in the Huainan mining area. *Environmental Science and Pollution Research*, *29*(40), 60117–60132. https://doi.org/10.1007/s11356-022-19921-5

Zhang, Z., Zhou, H., Cao, H., Ji, J., Zhang, R., Li, W., Guo, H., Chen, L., Ma, C., Cui, M., Wang, J., Chen, H., Ding, G., Yan, C., Dong, L., Holmes, E. C., Meng, L., Hou, P., & Shi, W. (2022). Human-to-human transmission of Chlamydia psittaci in China, 2020: an epidemiological and aetiological investigation. *The Lancet Microbe*, *3*(7), e512–e520. https://doi.org/10.1016/S2666-5247(22)00064-7

APPENDICES

Appendix A: GEE Codes for Data Collection and NDVI Calculations

1. Nyambadwe

Data collection for Nyambadwe.

```
Imports (4 entries)
  var Nyambadwe: Table projects/ee-ibrahimassabie8/assets/Nyambadwe
  var s2: ImageCollection "Sentinel-2 MSI: MultiSpectral Instrument, Level-2A"
  var pre_cyclone: Image users/ibrahimassabie8/Nyambadwe_S2_oct2022 (26 bands)
  var post_cyclone: Image users/ibrahimassabie8/Nyambadwe_S2_oct2023 (26 bands)
```

PRE-CYLONE CODE

```
//1st step
// Center the map on Blantyre
Map.centerObject(Nyambadwe, 10);
// Add the shapefile to the map
Map.addLayer(Nyambadwe, {color: 'red'}, 'Nyambadwe Boundary');
// the time range
var startDate = '2022-10-01';
var endDate = '2022-10-30';
// Filtering the Sentinel-2 image collection by date and region
var filteredImages = s2
  .filterDate(startDate, endDate)
  .filterBounds(Nyambadwe)  //  images intersect
  .map(function(image) {
    return image.clip(Nyambadwe); // Clips images to the  shapefile
  });
//  the median image to reduce cloud cover
var finalImage = filteredImages.median();
// Display the final image on the map
Map.centerObject(Nyambadwe, 12);
Map.addLayer(finalImage, {bands: ['B4', 'B3', 'B2'], min: 0, max: 3000}, 'Final Image');
```

DATA EXPORTATION CODE FOR PRE-CYCLONE

```
// Export to Google Earth Engine Assets
Export.image.toAsset({
  image: finalImage,
  description: 'Nyambadwe_Sentinel2_oct2022_Asset',
  assetId: 'Nyambadwe_S2_oct2022', // GEE path
  scale: 10,
  region: Nyambadwe,
  maxPixels: 1e13
});

// Export to Google Drive
Export.image.toDrive({
  image: finalImage,
  description: 'Nyambadwe_Sentinel2_oct2022_Drive',
  folder: 'GEE_Exports', // Change to your preferred Google Drive folder
  fileNamePrefix: 'Nyambadwe_S2_oct2022',
  scale: 10,
  region: Nyambadwe,
  maxPixels: 1e13,
  fileFormat: 'GeoTIFF'
});
```

POST-CYLONE CODE

```
//2nd step
// Center the map on Blantyre
Map.centerObject(Nyambadwe, 10);
// Add the shapefile to the map
Map.addLayer(Nyambadwe, {color: 'red'}, 'Nyambadwe Boundary');

// Define the time range
var startDate = '2023-10-01';
var endDate = '2023-10-30';

// Filter the Sentinel-2 image collection by date and region
var filteredImages = s2
  .filterDate(startDate, endDate)
  .filterBounds(Nyambadwe)  // Eimages intersect with
  .map(function(image) {
    return image.clip(Nyambadwe); // Clips images to the  shapefile
  });

// Get the median image to reduce cloud cover
var finalImage = filteredImages.median();

// Display the final image on the map
Map.centerObject(Nyambadwe, 12);
Map.addLayer(finalImage, {bands: ['B4', 'B3', 'B2'], min: 0, max: 3000}, 'Final Image');
```

DATA EXPORTATION CODE FOR POST-CYCLONE

```
// Export to Google Earth Engine Assets
Export.image.toAsset({
  image: finalImage,
  description: 'Nyambadwe_Sentinel2_oct2023_Asset',
  assetId: 'Nyambadwe_S2_oct2023', // GEE asset path
  scale: 10,
  region: Nyambadwe,
  maxPixels: 1e13
});

// Export to Google Drive
Export.image.toDrive({
  image: finalImage,
  description: 'Nyambadwe_Sentinel2_oct2023_Drive',
  folder: 'GEE_Exports', // Google Drive folder
  fileNamePrefix: 'Nyambadwe_S2_oct2023',
  scale: 10,
  region: Nyambadwe,
  maxPixels: 1e13,
  fileFormat: 'GeoTIFF'
});
```

NDVI CODE FOR BOTH PRE AND POST CYCLONE

```
//3rd step
// Load stored assets for pre- and post-cyclone images
var pre_cyclone = ee.Image(pre_cyclone);
var post_cyclone = ee.Image(post_cyclone);

// Function to compute NDVI
function calculateNDVI(image) {
  return image.normalizedDifference(['B8', 'B4']).rename('NDVI');
}

// Compute NDVI for both time periods
var NDVI_pre = calculateNDVI(pre_cyclone);
var NDVI_post = calculateNDVI(post_cyclone);

// Visualization Parameters
var NDVIVis = {min: -1, max: 1, palette: ['blue', 'white', 'green']};

// Add NDVI layers to the map
Map.centerObject(Nyambadwe, 10);
Map.addLayer(NDVI_pre, NDVIVis, "NDVI Pre-Cyclone");
Map.addLayer(NDVI_post, NDVIVis, "NDVI Post-Cyclone");
```

EXPORTATION CODE FOR NDVI CALCULATION

```
// Export NDVI images
Export.image.toDrive({
  image: NDVI_pre,
  description: "NDVII_Nyambadwe_Pre_Cyclone",
  scale: 10,
  region: Nyambadwe,
  maxPixels: 1e13
});

Export.image.toDrive({
  image: NDVI_post,
  description: "Nyambadwe_Post_Cyclone",
  scale: 10,
  region: Nyambadwe,
  maxPixels: 1e13
});

// Export NDVI images to GEE Assets
Export.image.toAsset({
  image: NDVI_pre,
  description: "Nyambadwe_Pre_Cyclone_Asset",
  assetId: "NDVI1_Nyambadwe_Pre_Cyclone",
  scale: 10,
  region: Nyambadwe,
  maxPixels: 1e13
});

Export.image.toAsset({
  image: NDVI_post,
  description: "NDVI_Nyambadwe_Post_Cyclone_Asset",
  assetId: "NDVI_Nyambadwe_Post_Cyclone",
  scale: 10,
  region: Nyambadwe,
  maxPixels: 1e13
});
```

2. CHILOMONI

Data collection for Chilomoni.

```
Imports (4 entries)
  var Chilomoni: Table projects/ee-ibrahimassabie8/assets/Chilomoni
  var s2: ImageCollection "Sentinel-2 MSI: MultiSpectral Instrument, Level-1C"
  var pre_cyclone: Image users/ibrahimassabie8/Chilomoni_S2_oct2022 (19 bands)
  var post_cyclone: Image users/ibrahimassabie8/Chilomoni_S2_oct2023 (19 bands)
```

PRE-CYLONE CODE

```
//1st step
// Center the map on Blantyre
Map.centerObject(Chilomoni, 10);
// Add the shapefile to the map
Map.addLayer(Chilomoni, {color: 'red'}, 'Chilomoni Boundary');

// Define the time range
var startDate = '2022-10-01';
var endDate = '2022-10-30';

// Filter the Sentinel-2 image collection by date and region
var filteredImages = s2
  .filterDate(startDate, endDate)
  .filterBounds(Chilomoni)  // Ensures images intersect with
  .map(function(image) {
    return image.clip(Chilomoni); // Clips images to the  shapefile
  });

// Get the median image to reduce cloud cover
var finalImage = filteredImages.median();

// Display the final image on the map
Map.centerObject(Chilomoni, 12);
Map.addLayer(finalImage, {bands: ['B4', 'B3', 'B2'], min: 0, max: 3000}, 'Final Image');
```

DATA EXPORTATION CODE FOR PRE-CYCLONE

```
// Export to Google Earth Engine Assets
Export.image.toAsset({
  image: finalImage,
  description: 'Chilomoni_Sentinel2_oct2022_Asset',
  assetId: 'Chilomoni_S2_oct2022', // GEE asset path
  scale: 10,
  region: Chilomoni,
  maxPixels: 1e13
});

// Export to Google Drive
Export.image.toDrive({
  image: finalImage,
  description: 'Chilomoni_Sentinel2_oct2022_Drive',
  folder: 'GEE_Exports', // Google Drive folder
  fileNamePrefix: 'Chilomoni_S2_oct2022',
  scale: 10,
  region: Chilomoni,
  maxPixels: 1e13,
  fileFormat: 'GeoTIFF'
});
```

POST-CYLONE CODE

```
//2nd step
// Center the map on Blantyre
Map.centerObject(Chilomoni, 10);
// Add the shapefile to the map
Map.addLayer(Chilomoni, {color: 'red'}, 'Chilomoni Boundary');

// Define the time range
var startDate = '2023-09-01';
var endDate = '2023-09-30';

// Filter the Sentinel-2 image collection by date and region
var filteredImages = s2
  .filterDate(startDate, endDate)
  .filterBounds(Chilomoni)  // Ensures images intersect with
  .map(function(image) {
    return image.clip(Chilomoni); // Clips images to the  shapefile
  });

// Get the median image to reduce cloud cover
var finalImage = filteredImages.median();

// Display the final image on the map
Map.centerObject(Chilomoni, 12);
Map.addLayer(finalImage, {bands: ['B4', 'B3', 'B2'], min: 0, max: 3000}, 'Final Image');
```

DATA EXPORTATION CODE FOR POST-CYCLONE

```
// Export to Google Earth Engine Assets
Export.image.toAsset({
  image: finalImage,
  description: 'Chilomoni_Sentinel2_oct2023_Asset',
  assetId: 'Chilomoni_S2_oct2023', // GEE asset path
  scale: 10,
  region: Chilomoni,
  maxPixels: 1e13
});

// Export to Google Drive
Export.image.toDrive({
  image: finalImage,
  description: 'Chilomoni_Sentinel2_oct2023_Drive',
  folder: 'GEE_Exports', // Google Drive folder
  fileNamePrefix: 'Chilomoni_S2_oct2023',
  scale: 10,
  region: Chilomoni,
  maxPixels: 1e13,
  fileFormat: 'GeoTIFF'
});
```

NDVI CODE FOR BOTH PRE AND POST CYCLONE

```
// Load stored assets for pre- and post-cyclone images
var pre_cyclone = ee.Image(pre_cyclone);
var post_cyclone = ee.Image(post_cyclone);

// Function to compute NDVI
function calculateNDVI(image) {
  return image.normalizedDifference(['B8', 'B4']).rename('NDVI');
}

// Compute NDVI for both time periods
var NDVI_pre = calculateNDVI(pre_cyclone);
var NDVI_post = calculateNDVI(post_cyclone);

// Visualization Parameters
var NDVIVis = {min: -1, max: 1, palette: ['blue', 'white', 'green']};

// Add NDVI layers to the map
Map.centerObject(Chilomoni, 10);
Map.addLayer(NDVI_pre, NDVIVis, "NDVI Pre-Cyclone");
Map.addLayer(NDVI_post, NDVIVis, "NDVI Post-Cyclone");
```

EXPORTATION CODE FOR NDVI CALCULATION

```
// Export NDVI images
Export.image.toDrive({
  image: NDVI_pre,
  description: "NDVI_Chilomoni_Pre_Cyclone",
  scale: 10,
  region: Chilomoni,
  maxPixels: 1e13
});

Export.image.toDrive({
  image: NDVI_post,
  description: "Chilomoni_Post_Cyclone",
  scale: 10,
  region: Chilomoni,
  maxPixels: 1e13
});

// Export NDVI images to GEE Assets
Export.image.toAsset({
  image: NDVI_pre,
  description: "Chilomoni_Pre_Cyclone_Asset",
  assetId: "NDVI_Chilomoni_Pre_Cyclone",
  scale: 10,
  region: Chilomoni,
  maxPixels: 1e13
});

Export.image.toAsset({
  image: NDVI_post,
  description: "NDVI_Chilomoni_Post_Cyclone_Asset",
  assetId: "NDVI_Chilomoni_Post_Cyclone",
  scale: 10,
  region: Chilomoni,
  maxPixels: 1e13
});
```

3. Soche_Chilobwe

Data collection.

```
Imports (4 entries)
  var s2: ImageCollection "Sentinel-2 MSI: MultiSpectral Instrument, Level-2A"
  var Soche_Chilobwe: Polygon, 19 vertices
  var post_cyclone: Image users/ibrahimassabie8/Soche_Chilobwe_S2_OCT2023 (26 bands)
  var pre_cyclone: Image users/ibrahimassabie8/Soche_Chilobwe_S2_oct2022 (26 bands)
```

PRE-CYLONE CODE

```
//1st step
// Center the map on Blantyre
Map.centerObject(Soche_Chilobwe, 10);
// Add the shapefile to the map
Map.addLayer(Soche_Chilobwe, {color: 'red'}, 'Soche_Chilobwe Boundary');

// Define the time range
var startDate = '2022-10-01';
var endDate = '2022-10-30';

// Filter the Sentinel-2 image collection by date and region
var filteredImages = s2
  .filterDate(startDate, endDate)
  .filterBounds(Soche_Chilobwe)  //  images intersect with
  .map(function(image) {
    return image.clip(Soche_Chilobwe); // Clips images to the  shapefile
  });

// Get the median image to reduce cloud cover
var finalImage = filteredImages.median();

// Display the final image on the map
Map.centerObject(Soche_Chilobwe, 12);
Map.addLayer(finalImage, {bands: ['B4', 'B3', 'B2'], min: 0, max: 3000}, 'Final Image');

```

DATA EXPORTATION CODE FOR POST-CYCLONE

```
// Export to Google Earth Engine Assets
Export.image.toAsset({
  image: finalImage,
  description: 'Soche_Chilobwe_Sentinel2_oct2022_Asset',
  assetId: 'Soche_Chilobwe_S2_oct2022', //  GEE asset path
  scale: 10,
  region: Soche_Chilobwe,
  maxPixels: 1e13
});

// Export to Google Drive
Export.image.toDrive({
  image: finalImage,
  description: 'Soche_Chilobwe_Sentinel2_oct2022_Drive',
  folder: 'GEE_Exports', // Google Drive folder
  fileNamePrefix: 'Soche_Chilobwe_S2_oct2022',
  scale: 10,
  region: Soche_Chilobwe,
  maxPixels: 1e13,
  fileFormat: 'GeoTIFF'
});

```

POST-CYLONE CODE

```
//2nd step
// Center the map on Blantyre
Map.centerObject(Soche_Chilobwe, 10);
// Add the shapefile to the map
Map.addLayer(Soche_Chilobwe, {color: 'red'}, 'Soche_Chilobwe Boundary');

// Define the time range
var startDate = '2023-10-01';
var endDate = '2023-10-30';

// Filter the Sentinel-2 image collection by date and region
var filteredImages = s2
  .filterDate(startDate, endDate)
  .filterBounds(Soche_Chilobwe)  // Ensures images intersect with Ndirande
  .map(function(image) {
    return image.clip(Soche_Chilobwe); // Clips images to the Ndirande shapefile
  });

// Get the median image to reduce cloud cover
var finalImage = filteredImages.median();

// Display the final image on the map
Map.centerObject(Soche_Chilobwe, 12);
Map.addLayer(finalImage, {bands: ['B4', 'B3', 'B2'], min: 0, max: 3000}, 'Final Image');

```

DATA EXPORTATION CODE FOR POST-CYCLONE

```
// Export to Google Earth Engine Assets
Export.image.toAsset({
  image: finalImage,
  description: 'Soche_Chilobwe_Sentinel2_OCT2023_Asset',
  assetId: 'Soche_Chilobwe_S2_OCT2023', //  GEE asset path
  scale: 10,
  region: Soche_Chilobwe,
  maxPixels: 1e13
});

// Export to Google Drive
Export.image.toDrive({
  image: finalImage,
  description: 'Soche_Chilobwe_Sentinel2_OCT2023_Drive',
  folder: 'GEE_Exports', // CGoogle Drive folder
  fileNamePrefix: 'Soche_Chilobwe_S2_OCT2023',
  scale: 10,
  region: Soche_Chilobwe,
  maxPixels: 1e13,
  fileFormat: 'GeoTIFF'
});
```

NDVI CODE FOR BOTH PRE AND POST CYCLONE

```
// Load stored assets for pre- and post-cyclone images
var pre_cyclone = ee.Image(pre_cyclone);
var post_cyclone = ee.Image(post_cyclone);

// Function to compute NDVI
function calculateNDVI(image) {
  return image.normalizedDifference(['B8', 'B4']).rename('NDVI');
}

var pre_cyclone = ee.Image(pre_cyclone);
var post_cyclone = ee.Image(post_cyclone);

// Function to compute NDVI
function calculateNDVI(image) {
  return image.normalizedDifference(['B8', 'B4']).rename('NDVI');
}

// Compute NDVI for both time periods
var NDVI_pre = calculateNDVI(pre_cyclone);
var NDVI_post = calculateNDVI(post_cyclone);

// Visualization Parameters
var NDVIVis = {min: -1, max: 1, palette: ['blue', 'white', 'green']};

// Add NDVI layers to the map
Map.centerObject(Soche_Chilobwe, 10);
Map.addLayer(NDVI_pre, NDVIVis, "NDVI Pre-Cyclone");
Map.addLayer(NDVI_post, NDVIVis, "NDVI Post-Cyclone");
```

EXPORTATION CODE FOR NDVI CALCULATION

```
// Export NDVI images
Export.image.toDrive({
  image: NDVI_pre,
  description: "NDVI_Soche_Chilobwe_Pre_Cyclone",
  scale: 10,
  region: Soche_Chilobwe,
  maxPixels: 1e13
});

Export.image.toDrive({
  image: NDVI_post,
  description: "NDVI_Soche_Chilobwe_Post_Cyclone",
  scale: 10,
  region: Soche_Chilobwe,
  maxPixels: 1e13
});

// Export NDVI images to GEE Assets
Export.image.toAsset({
  image: NDVI_pre,
  description: "NDVI_Soche_Chilobwe_Pre_Cyclone_Asset",
  assetId: "NDVI_Soche_Chilobwe_Pre_Cyclone",
  scale: 10,
  region: Soche_Chilobwe,
  maxPixels: 1e13
});

Export.image.toAsset({
  image: NDVI_post,
  description: "NDVI_Soche_Chilobwe_Post_Cyclone_Asset",
  assetId: "NDVI_Soche_Chilobwe_Post_Cyclone",
  scale: 10,
  region: Soche_Chilobwe,
  maxPixels: 1e13
});
```

4. Ndirande

Data collection.

```
Imports (4 entries)
  var Ndirande: Table projects/ee-ibrahimassabie8/assets/Ndirande
  var s2: ImageCollection "Sentinel-2 MSI: MultiSpectral Instrument, Level-2A"
  var pre_cyclone: Image users/ibrahimassabie8/Ndirande_S2_oct2022 (26 bands)
  var post_cyclone: Image users/ibrahimassabie8/Ndirande_S2_oct2023 (26 bands)
```

PRE-CYLONE CODE

```
//1st step
// Center the map on Blantyre
Map.centerObject(Ndirande, 10);
// Add the shapefile to the map
Map.addLayer(Ndirande, {color: 'red'}, 'Ndirande Boundary');

// Define the time range
var startDate = '2022-10-01';
var endDate = '2022-10-30';

// Filter the Sentinel-2 image collection by date and region
var filteredImages = s2
  .filterDate(startDate, endDate)
  .filterBounds(Ndirande)  // Ensures images intersect with Ndirande
  .map(function(image) {
    return image.clip(Ndirande); // Clips images to the Ndirande shapefile
  });

// Get the median image to reduce cloud cover
var finalImage = filteredImages.median();

// Display the final image on the map
Map.centerObject(Ndirande, 12);
Map.addLayer(finalImage, {bands: ['B4', 'B3', 'B2'], min: 0, max: 3000}, 'Final Image');
```

DATA EXPORTATION CODE FOR POST-CYCLONE

```
// Export to Google Earth Engine Assets
Export.image.toAsset({
  image: finalImage,
  description: 'Ndirande_Sentinel2_oct2022_Asset',
  assetId: 'Ndirande_S2_oct2022', // GEE asset path
  scale: 10,
  region: Ndirande,
  maxPixels: 1e13
});

// Export to Google Drive
Export.image.toDrive({
  image: finalImage,
  description: 'Ndirande_Sentinel2_oct2022_Drive',
  folder: 'GEE_Exports', //  Google Drive folder
  fileNamePrefix: 'Ndirande_S2_oct2022',
  scale: 10,
  region: Ndirande,
  maxPixels: 1e13,
  fileFormat: 'GeoTIFF'
});
```

POST-CYLONE CODE

```
//2nd step
// Center the map on Blantyre
Map.centerObject(Ndirande, 10);
// Add the shapefile to the map
Map.addLayer(Ndirande, {color: 'red'}, 'Ndirande Boundary');

// Define the time range
var startDate = '2023-10-01';
var endDate = '2023-10-30';

// Filter the Sentinel-2 image collection by date and region
var filteredImages = s2
  .filterDate(startDate, endDate)
  .filterBounds(Ndirande)  // Ensures images intersect with Ndirande
  .map(function(image) {
    return image.clip(Ndirande); // Clips images to the Ndirande shapefile
  });

// Get the median image to reduce cloud cover
var finalImage = filteredImages.median();

// Display the final image on the map
Map.centerObject(Ndirande, 12);
Map.addLayer(finalImage, {bands: ['B4', 'B3', 'B2'], min: 0, max: 3000}, 'Final Image');

```

DATA EXPORTATION CODE FOR POST-CYCLONE

```
// Export to Google Earth Engine Assets
Export.image.toAsset({
  image: finalImage,
  description: 'Ndirande_Sentinel2_oct2023_Asset',
  assetId: 'Ndirande_S2_oct2023', //  GEE asset path
  scale: 10,
  region: Ndirande,
  maxPixels: 1e13
});

// Export to Google Drive
Export.image.toDrive({
  image: finalImage,
  description: 'Ndirande_Sentinel2_oct2023_Drive',
  folder: 'GEE_Exports', // Google Drive folder
  fileNamePrefix: 'Ndirande_S2_oct2023',
  scale: 10,
  region: Ndirande,
  maxPixels: 1e13,
  fileFormat: 'GeoTIFF'
});

```

NDVI CODE FOR BOTH PRE AND POST CYCLONE

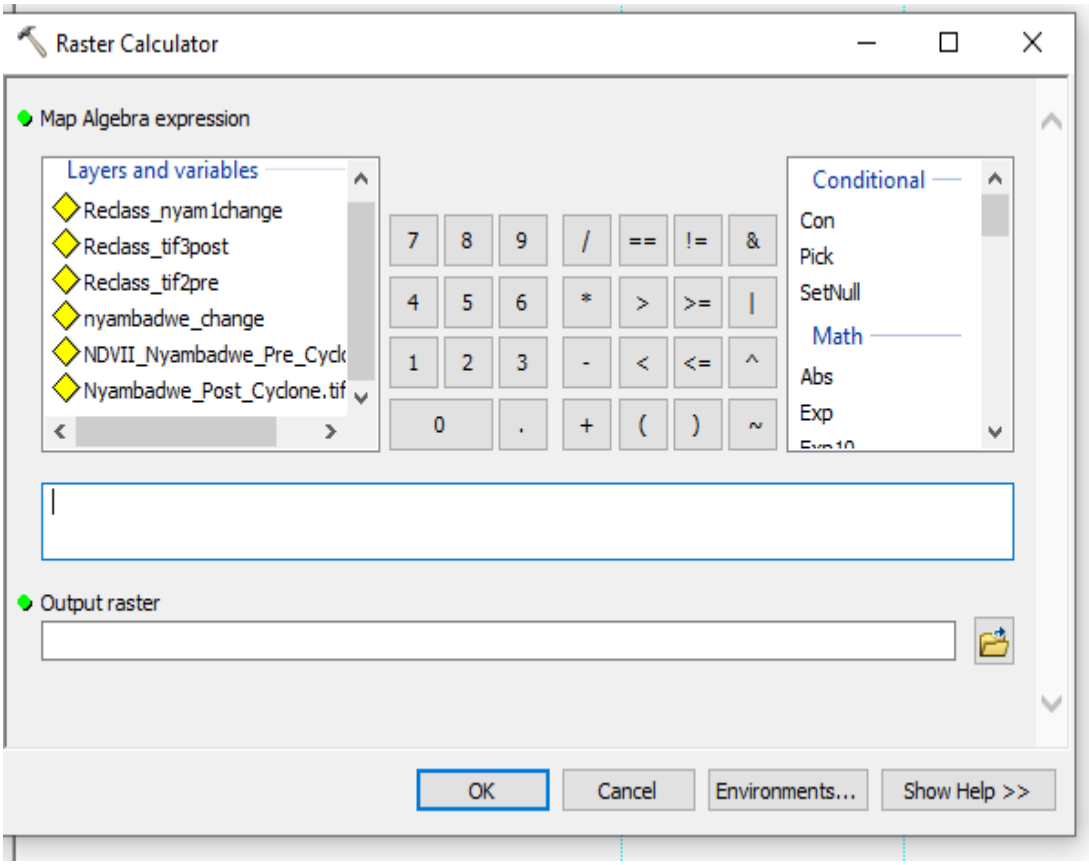
```
101
102 //3rd step
103 var pre_cyclone = ee.Image(pre_cyclone);
104 var post_cyclone = ee.Image(post_cyclone);
105
106 // Function to compute NDVI
107 function calculateNDVI(image) {
108   return image.normalizedDifference(['B8', 'B4']).rename('NDVI');
109 }
110
111 // Compute NDVI for both time periods
112 var NDVI_pre = calculateNDVI(pre_cyclone);
113 var NDVI_post = calculateNDVI(post_cyclone);
114
115 // Visualization Parameters
116 var NDVIVis = {min: -1, max: 1, palette: ['blue', 'white', 'green']};
117
118 // Add NDVI layers to the map
119 Map.centerObject(Ndirande, 10);
120 Map.addLayer(NDVI_pre, NDVIVis, "NDVI Pre-Cyclone");
121 Map.addLayer(NDVI_post, NDVIVis, "NDVI Post-Cyclone");
122
```

EXPORTATION CODE FOR NDVI CALCULATION

```
123 // Export NDVI images
124 Export.image.toDrive({
125   image: NDVI_pre,
126   description: "NDVI_Ndirande_Pre_Cyclone",
127   scale: 10,
128   region: Ndirande,
129   maxPixels: 1e13
130 });
131
132 Export.image.toDrive({
133   image: NDVI_post,
134   description: "NDVI_Ndirande_Post_Cyclone",
135   scale: 10,
136   region: Ndirande,
137   maxPixels: 1e13
138 });
139
140 // Export NDVI images to GEE Assets
141 Export.image.toAsset({
142   image: NDVI_pre,
143   description: "NDVI_Ndirande_Pre_Cyclone_Asset",
144   assetId: "NDVI_Ndirande_Pre_Cyclone",
145   scale: 10,
146   region: Ndirande,
147   maxPixels: 1e13
148 });
149
150 Export.image.toAsset({
151   image: NDVI_post,
152   description: "NDVI_Ndirande_Post_Cyclone_Asset",
153   assetId: "NDVI_Ndirande_Post_Cyclone",
154   scale: 10,
155   region: Ndirande,
156   maxPixels: 1e13
157 });
158
```

Appendix B: ArcMap Raster Calculator Expression for NDVI Change Detection

The NDVI change detection map was generated in ArcMap using the Raster Calculator with the following expression:



"PostCyclone_NDVI.tif" - "PreCyclone_NDVI.tif"

where:

PostCyclone_NDVI.tif represents the post-cyclone NDVI raster.

PreCyclone_NDVI.tif represents the pre-cyclone NDVI raster.

Appendix C: Summary of Satellite Data Collection Parameters

Parameter	Description
Satellite Data Source	Sentinel-2 MSI Level-2A https://developers.google.com/earth-engine/datasets/catalog/COPERNICUS_S2_HARMONIZED
Bands Used	Band 4 (Red), Band 8 (Near Infrared)
Spatial Resolution	10 meters for core analysis bands
Cloud Cover	Less than 10%
Pre-Cyclone Period	01-10-2022 - 30-10-2022
Post-Cyclone Period	01-10-2023 - 30-10-2023
Study Areas (AOIs)	Nyambadwe, Chilomoni, Soche-Chilobwe, Ndirande
Data Access Platform	GEE https://code.earthengine.google.com/
Exported Outputs	- Pre-Cyclone NDVI GeoTIFF - Post-Cyclone NDVI GeoTIFF - NDVI Change GeoTIFF